Identification of a novel RNA modifications-related model to improve bladder cancer outcomes in the framework of predictive, preventive, and personalized medicine

Ziying Zhang
Sun Yat-sen University Cancer Center
Peng Chen
Sun Yat-sen University Cancer Center
Fangyi Liu
Sun Yat-sen University Cancer Center
Censhan Lin
Sun Yat-sen University Cancer Center
Ru Deng
Sun Yat-sen University Cancer Center
Liyan Wu
Sun Yat-sen University Cancer Center
Yun Cao
Sun Yat-sen University Cancer Center
Jingping Yun
Sun Yat-sen University Cancer Center
Yuhua Huang (huangyh@sysucc.org.cn)
Sun Yat-sen University Cancer Center https://orcid.org/0000-0001-8340-3582

Research Article

Keywords: Predictive preventive personalized medicine (PPPM/3PM), RNA modification, bladder cancer, prognostic model, patient stratification, immunotherapy efficacy

Posted Date: April 14th, 2022

DOI: https://doi.org/10.21203/rs.3.rs-1452102/v1

Abstract

Background

Bladder cancer (BCa) is the leading reason for death among malignancies in genitourinary system. RNA modifications participate in pivotal tumor-promoting mechanisms in specific epigenetic contexts. Our study aimed to propose a novel model associated with the “writer” enzymes of five primary RNA adenosine modifications (including m^6A, m^6A_m, m^1A, alternative polyadenylation, and adenosine-to-inosine editing), which could predict the clinical outcome and immunotherapeutic efficacy of BCa, thus conferring a promising orientation for BCa predictive, preventive, and personalized medicine (PPPM/3PM).

Methods

Unsupervised clustering was employed to categorize BCa into different RNA modification patterns on the basis of gene expression profiles of 34 RNA modification “writers”. The RNA modification “writers” score (RMS) signature composed of RNA phenotype-associated differentially expressed genes (DEGs) was established using the least absolute shrinkage and selection operator (LASSO). The prognostic power of the RMS model was evaluated using Kaplan-Meier analysis and receiver operating characteristic curves. A visualized nomogram was established for BCa risk stratification. The potential applicability of the RMS model in predicting the therapeutic responsiveness was assessed through the Genomics of Drug Sensitivity in Cancer database and multiple immunotherapy datasets.

Results

Two distinct RNA modification patterns were determined among 1410 BCa samples, showing radically varying clinical outcomes and biological characteristics. The RMS model comprising 14 RNA modification phenotype-associated prognostic DEGs was positively correlated with the unsatisfactory outcome of BCa patients in a meta-GEO training cohort (HR = 3.00, 95% CI = 2.19–4.12) and the TCGA-BLCA validation cohort (HR = 1.53, 95% CI = 1.13–2.09). The infiltration of immunosuppressive cells and the activation of EMT, angiogenesis, IL-6/JAK/STAT3 signaling were markedly enriched in RMS-high cohort. A nomogram including age, N classification and the RMS exhibited high prognostic prediction accuracy, with a concordance index of 0.745. The combination of the RMS model and conventional characteristics (TMB, TNB and PD-L1) achieved an optimal area under the curve of 0.828 in differentiating responders from non-responders to immunotherapy based on IMvigor210 cohort.

Conclusion

Our report conferred the first landscape of five forms of RNA modifications in BCa and emphasized the excellent power of the RNA modifications-related model in evaluating prognosis and immunotherapeutic efficacy. In accordance with our model, physicians can not only conduct early identification of high-risk patients to confer them with priority attention and targeted prevention, but also judge patients' responses to immunotherapy in advance to render personalized therapy, which is conducive to the research and practice of PPPM/3PM in BCa.

1. Introduction

1.1 Epidemiology and etiology of bladder cancer

BCa is a common malignancy in women and is the fourth most diagnosed malignancy in men globally, with an estimated 500000 new cases and 200000 deaths annually [1–3]. Advanced age [4], the male [5], exposure to tobacco smoke [6], chronic inflammatory status [7], pelvic radiation [8], usage of cyclophosphamide [9], and genetic or epigenetic alterations [10] contribute to the tumorigenesis and development of BCa. Currently, epigenetic mechanisms implicated in cancer-associated genes and inflammatory genes have gradually been becoming the center of BCa etiology research [11]. Epigenetics refers to heritable changes in a cellular phenotype caused by chromosomal alterations that is independent of changes in DNA sequence [12]. Researches concerning RNA editing, splicing, polyadenylation, and post-transcription are advancing rapidly, thus providing an additional lens through which the essential effects of RNA modifications (also called RNA epigenetics) on modulating BCa development can be unraveled [13, 14].

1.2 Effects of five forms of RNA modifications in host physiology and cancers

In human cells, RNA modification exists in all nucleotides: A, U, C, and G [15]. RNA harbors exceeding 170 forms of chemical modifications, such as N^6-methyladenosine (m^6A), N^6,2'-O-dimethyladenosine (m^6A_m), N^1-methyladenosine (m^1A), N^7-methylguanosine (m^7G), and alternative polyadenylation (APA) [16]. As reported, a direct and mutual interplay exists among these modifications. One of the best-characterized examples is that inhibition of m^6A-catalyzing enzymes leads to global adenosine-to-inosine (A-to-I) editing alterations potentially via a disturbance of RNA secondary structure essential for the deamination [17, 18]. Moreover, a novel molecular axis METTL3/ADAR1/CDK2 conjoining m^6A and A-to-I that can forcefully alter the scenario of post-transcriptional events and ultimately exerts a pro-oncogenic effect in glioblastoma [19]. Concerning that we are incapable of underlining all types of RNA modifications in our report and adenine is a kind of RNA nucleotide with the most widespread chemical diversities, herein, we primarily concentrated on adenine-associated RNA modifications (m^6A, m^6A_m, m^1A, APA and A-to-I editing). Above modifications are commonly generated through the activity of enzymes referred to as "writers" [20].

m^6A is defined as the methylation occurring at the sixth nitrogen atom of adenine base, which is the most plentiful and better characterized internal RNA modification form in eukaryotic cells [21, 22]. This modification is catalyzed via m^6A-methyltransferases complex, including METTL3, METTL14, RBM15, WTAP, VIRMA, ZC3H13, METTL16, CBLL1, and RBM15B [23, 24]. The presence of m^6A not only influences RNA stability, translational efficiency, and epigenetic function of non-coding RNAs, but also exerts crucial effect on circadian rhythm maintenance and cell cycle modulation, cell differentiation and reprogramming, embryonic stem cell self-renewal, T cell homeostasis, neuronal functions, tumorigenicity and metastasis [16, 25].

2'-O-methyladenosine (Am) (as the first nucleotide adjacent to m^7G cap) is subsequently methylated at the N^6 position to convert into m^6A_m RNA modification, which is generally mediated by methyltransferase (including PCIF1 and METTL4) [26–28]. m^6A_m, known as the second most abundant modification in cellular mRNAs and small nuclear RNAs (snRNAs), probably participates in tumor development through modulating RNA splicing, mRNA stability and cap-dependent translation [16]. Specifically, METTL4 as a novel internal m^6A_m methyltransferase for U2 snRNA in human has the capacity to catalyze Am at U2 snRNA position 30 into m^6A_m, loss of which broadly impacts various biological pathways, including RNA splicing and cell proliferation [27, 29, 30].

m^1A can be defined as a reversible modification in tRNA, rRNA, mRNA, lncRNA and mitochondrial transcripts, affecting the first nitrogen atom of adenine base [31–33]. Multiple m^1A-methyltransferases as "writers" have been revealed, including TRMT6/61A/61B, TRMT10C, and RRP8 [34]. The electro-chemical crosstalk caused by positive electrostatic charge of m^1A can maintain normal function and structure of tRNA. Additionally, m^1A fosters the translation initiation and tertiary structure of ribosomes while restrains most reverse transcription of RNA, thus modulating the onset and development of diseases [35].

APA is a phenomenon that nascent mRNA is cleaved at diverse sites, followed by addition of a poly (A) tail, and further generate multifarious transcript isoforms with diverse lengths of 3'-untranslated region (3'UTR) [36, 37]. The APA of mRNAs is elicited by multiple subcomplexes, namely CPSF, CSTF, WDR33, FIP1L1, PCF11, CLP1, and PABPN1 [38–41]. Because 3'UTR accommodates microRNA (miRNA)-binding sites, APA event is implicated in mRNA stability, translation, and cellular localization. Extensive shortening of 3'UTR has been revealed in a wide variety of tumors, which enables the activation of oncogenes or restrains tumor-suppressor genes in trans through a perturbation of competing endogenous RNA (ceRNA) network, thereby facilitating tumorigenesis [42–44]. Disturbance in the expression of APA factors is also detected in diverse malignant tumors, leading to abnormal usage of proximal polyA sites (PAS) [45, 46].

A-to-I editing is one of the most abundant RNA modification events affecting adenosine in humans, where adenosine deaminase acting on RNA (ADAR) enzymes (including ADAR, ADARB1, and ADARB2) shift adenosine nucleotides towards inosines through the deamination and eventually lead to specific nucleotide alterations at RNA level and changes in the sequence of amino acids in protein without

influencing DNA sequence [17, 47, 48]. A previous study has reported that A-to-I-edited miR-376a-3p is diminished in glioblastoma, thereby accelerating tumor invasiveness [49]. ADARB1-mediated endogenous and exogenous A-to-I editing in miR-379-5p suppresses tumor proliferation through targeting the apoptosis promoter CD97 [50]. A-to-I RNA editing in RHOQ is sufficient to confer more aggressive tumor behavior in colorectal cancer [51]. Therefore, A-to-I editing is essential for neoplasia and progressive peculiarity of tumor through modulating site-specific modifications of tumor-associated molecules.

1.3 Potential association between RNA modifications and immune, immunotherapy

Above five classes of RNA modification “writers” potentially constitute a fundamental and sophisticated regulatory network in BCa, and a thorough comprehending of the network potentially confers a novel insight into the contribution of RNA modification to BCa tumorigenesis. Immune-checkpoint blockade (ICB) is currently on the cutting edge and profiled as the most promising immunotherapeutic strategy in tumor. High tumor mutation burden (TMB) of BCa renders it susceptible to ICB therapy, specifically for monoclonal antibodies targeted programmed cell death-1 (PD-1) and its ligand, PD-L1. Nevertheless, merely lower than 30% of BCa patients yield an objective response from ICB [52, 53]. Thus, the ideal approach to screening a cluster of BCa patients who will experience optimal response to the frontline immunotherapy remains to be determined, one of which is to deeply analyze the tumor microenvironment (TME) and mechanism underlying the low response rate to ICB. Compelling and accumulating evidence has demonstrated the crosstalk between immune cells infiltrating in the TME and mRNA modification and associated enzymes. For example, METTL3 deficiency results in the upregulation of IRAKM and subsequently suppresses TLR4 signaling, thus inhibiting macrophage activation [54]. METTL3 can modulate T cell homeostatic proliferation through targeting IL-7/STAT5/SOCS pathway [55]. METTL3-mediated m^6A modification also facilitates the translation of CD40, CD80 and cytokine IL-12 transcripts to accelerate dendritic cell (DC) activation [56]. Thus, RNA modification “writers” are increasingly recognized as an orchestrator to influence homeostasis and function of immune cells in the host. Nevertheless, current studies have principally concentrated on single RNA modification “writer” on account of methodological limitations, while a highly coordinated interaction of various tumor-inhibiting factors is responsible for the antitumor effect of these RNA modification regulators [57]. Thus, a penetrating investigation of dynamic functional network composed of RNA modification regulators and TME components is of extraordinary significance to exploit better strategies for cancer immunotherapy.

1.4 Working hypotheses

We hypothesize that five types of RNA adenosine modifications (m^6A, m^6Am, m^1A, APA, and A-to-I editing) exert a crucial effect on the clinical outcome, TME, chemotherapeutic sensitivity and immunotherapeutic efficacy of BCa. The RNA modifications-related model potentially develops into a promising signature to guide the prognosis prediction, patient stratification, personalized medical services of BCa patients, ultimately facilitating the optimization of predictive, preventive, and personalized medicine (PPPM/3PM) for BCa.

1.5 Study design

In our study, we firstly incorporated 1410 cases from eight independent BCa datasets to determine RNA modification patterns through unsupervised clustering of gene-expression profiles of 34 RNA modification “writers” and further correlated RNA modification pattern with the prognosis of BCa and the infiltrating characteristics of multiple immune cells in the TME. Secondly, on the basis of DEGs between distinct RNA modification patterns, we established the RMS model to individually evaluate the performance of “writers”. Additionally, we assessed the immune infiltration landscape and presented potential carcinogenic mechanisms in BCa individuals with high risk score. Furthermore, a nomogram-based risk evaluation and clinicopathological characteristics of cases were developed to enhance the predictive power and accuracy. Ultimately, we revealed the applicability of the RMS model to differentiate the post-transcriptional events, and depicted its predictive efficiency in assessing patients’ responsiveness to chemotherapy drugs and ICBs.

1.6 Expected impacts in the context of predictive, preventive, and personalized medicine

The PPPM/3PM is currently recognized as an optimal strategy to pursuit greater benefits from healthcare and disease care fields, which is endowed with the capacity to predict personal predisposition to disease, confer pertinent intervention and prevention measures, and formulate individualized treatment programs, thereby making great contributions to curing intractable diseases, improving human health, and decreasing medical expenditure [58–61]. The complexity and heterogeneity of the TME result in varying clinical outcomes and responsiveness to therapy of BCa patients [62]. In the PPPM/3PM framework, the elucidation for underlying molecular characteristics of diseases, the screening for prognostic biomarkers and the establishment of clinically available and precise predictive models are of great importance for facilitating the optimization of individualized medical intervention [63]. Remarkable progress in high throughput sequencing permits the intensive investigations of cancer mechanisms, which confers precise screening biomarkers via multi-parameter systematic strategy, and effectively proposes preventive and predictive therapy measures, ultimately bringing light to the implementation of the PPPM/3PM paradigm for BCa [64]. In this study, based on bioinformatic analysis of high-throughput data, the establishment of a powerful RNA modifications-associated signatures can not only effectively predict the prognosis of BCa, but also distinguish a subset of responsive patients who will benefit from immunotherapy in the whole research population, which potentially contributes to the advancement of medical standard of PPPM/3PM medicine concepts [65].

2. Materials And Methods

2.1 Data extraction and preprocessing

The program flowchart of our report was illustrated in **Figure S1**. The public somatic mutation information for 412 BCa samples (workflow type: VarScan2 Variant Aggregation and Masking) was

downloaded from The Cancer Genome Atlas-Bladder Urothelial Carcinoma (TCGA-BLCA) (https://portal.gdc.cancer.gov/repository). The somatic copy number variation (CNV) status for 409 BCa cases, and the RNA-sequencing (RNA-seq) data and corresponding clinical datasheets for 411 BCa tissues were extracted from the University of California Santa Cruz (UCSC) Xena browser (https://xenabrowser.net). The clinicopathologic parameters included age, gender, T, N, M classification, tumor stage, histological grade, overall survival (OS) and survival status. RNA-seq data (FPKM values) were further converted into TPM values to make samples more comparable. The waterfall plot that depicted the mutant landscape of TCGA-BLCA cohort was established through “maftools” R package [66].

Additionally, the gene expression profiles and detailed clinical annotations of eight BCa-associated Gene-Expression Omnibus (GEO) cohorts were extracted from the supplementary files of original manuscript or downloaded from http://www.ncbi.nlm.nih.gov/geo/ through “GEOquery” R package [67], including GSE13507 based on platform GPL6102 (with 188 BLCA samples) [68, 69], GSE32894 based on platform GPL6947 (with 308 BLCA samples) [70], GSE32548 based on platform GPL6947 (with 131 BLCA samples) [71], GSE128959 based on platform GPL6244 (with 200 BLCA samples) [72], GSE31684 based on platform GPL570 (with 93 BLCA samples) [73, 74], GSE48075 based on platform GPL6947 (with 142 BLCA samples) [75, 76], GSE104922 based on platform GPL6244 (with 41 BLCA samples) [77], GSE83586 based on platform GPL6244 (with 307 BLCA samples) [78]. The ComBat algorithm of “sva” R Package was utilized for eliminating the batch effects caused by non-biological technical biases [79]. Eventually, these data from above GEO sets were united into a meta-GEO group (including 1410 BCa patients) to formulate our RMS model.

2.2 Weighted gene co-expression network analysis (WGCNA)

WGCNA can be employed to illuminate the relationship between gene networks modules and clinical phenotype at transcriptome level based on data reduction method and unsupervised classification method [80]. Firstly, the soft threshold power was estimated using nearly scale-free topology to construct a scale-free network. The distance between each gene pair was identified in accordance with the toplogical overlap matrix similarity. Furthermore, hierarchical clustering analysis with the average method and dynamic method was utilized to establish the cluster tree and stratify a variant set of genes into different modules, respectively, respectively. The branches of the cluster tree labeled with a specific color signified one module comprising genes with high correlation. Modules were merged on the condition that their correlation of module eigengene (ME) was over 0.75, implying the similarity of their expression profiles. Pearson’s correlation coefficients and the corresponding P values was applied for assessing the correlation between MEs and clinical traits, such as tumor stage, histological grade, and survival status. By convention, one module with the greatest absolute of module significance (MS) was chosen for subsequent analysis. For each module, module membership (MM) was characterized with the correlation coefficient between ME and gene expression profile. Gene Significance (GS) value was applied to quantify the correlation between individual gene and clinical factors [80]. Genes with MM > 0.8 and | GS | > 0.2 were defined as hub genes in the module. In our study, the “WGCNA” R package was performed to

establish a co-expression network of 5657 prognosis-associated genes in 411 BCa patients with clinicopathological parameters [81].

2.3 Immunohistochemistry (IHC)

Samples were collected from BCa cases who conformed to the following criteria: (1) Patients were clinically and pathologically diagnosed with BCa; (2) None of cases was performed by radiotherapy or chemotherapy before surgery; (3) Paired adjacent non-neoplastic bladder tissues were available for contrast. All tissues were acquired from Sun Yat-sen University Cancer Center and immediately fixed with formalin. The samples were embedded in paraffin for the construction of tissue microarray (TMA) that included 84 paired BCa samples. Prior to participating in this study, all patients received written informed consent. The project was approved by the Ethics Committee of Sun Yat-sen University Cancer Center.

The BCa TMA was dewaxed with xylene and further blocked endogenous peroxidase activity in 3% hydrogen peroxide solution. Antigen retrieval was conducted through boiling the samples in sodium-citrate buffer (pH 6.0) for 3 min. The TMA was incubated overnight with primary antibodies (anti-KIAA1429: 1:500, # 25712-1-AP, Proteintech, USA; anti-IFNLR1: 1:100, # ab224395, Abcam, USA) at 4℃ overnight. After incubating with secondary antibody at room temperature for 30 min, the TMA was counter-stained with hematoxylin, dehydrated and covered. The degree of immunostaining of the TMA was evaluated by two independent pathologists blinded to the histopathological characteristics of the samples. The proportion of positively stained cells was scored on a scale of 0–4 (0%, 1–25%, 26–50%, 51–75%, and 76–100%). The staining intensity was scored with four scoring levels: 0 (negative), 1 (weak), 2 (medium) and 3 (strong). The staining score was staining by multiplying the proportion of positively stained cells with the intensity score. The total scores were relatively stratified into three grades, < 3 scores, 3 to 6 scores, and > 6 scores, which corresponded to negative, weak positive and strong positive staining, respectively.

2.4 Collection of clinical datasets with immunotherapy

Three immunotherapeutic cohorts with accessible genomic/transcriptomic data and sufficient clinical annotations were enrolled into our report to investigate the association between the RMS and efficacy of immunotherapy: (1) IMvigor210 cohort, advanced urothelial carcinoma (UC) with atezolizumab (anti-PD-L1 antibody) treatment [82]; (2) Snyder UC cohort, patients with locally advanced or metastatic UC treated with atezolizumab [83]; (3) Montoya melanoma cohort, advanced melanoma patients underwent MAGE-3 antigen-based immunotherapy [84].

For IMvigor210 cohort, according to the Creative Commons 3.0 License, the gene expression data and detailed clinical annotation were downloaded from http://research-pub.gene.com/IMvigor210CoreBiologies. The raw data were normalized through “edgeR” R package and were subsequently converted to TPM values. Similarly, data of Snyder UC cohort were extracted from http://doi.org/10.5281/zenodo.546110. Furthermore, RNA-seq and clinical information from Montoya melanoma cohort were deposited in GSE35640 (N = 55).

2.5 Unsupervised clustering analysis of RNA modification “writers”

To identify the optimal number of clusters, we utilized unsupervised consensus hierarchical clustering algorithm through “ConsensuClusterPlus” R package, to perform clustering analysis of 34 RNA modification “writers” of 1410 BCa samples in the meta-GEO cohort [85]. The robustness of above stratification was identified via the consensus clustering algorithm with 1000 times repetitions.

2.6 Gene set variation analysis (GSVA) and Gene Ontology (GO) analysis

GSVA was conducted using “GSVA” R package, thus depicting the differences in the enrichment of signaling pathways between diverse RNA modification patterns [86]. The well-acknowledged biological signatures were acquired from the Hallmarker gene set [curated from the Molecular Signature Database (MSigDB) v7.1] [87] and Mariathasan *et al.* established gene set (download from http://research-pub.gene.com/IMvigor210CoreBiologies) [82]. GO functional annotation for 34 RNA modification enzyme genes were identified through “clusterProfiler” R package with a threshold of false discovery rate (FDR) < 0.05 [81, 88].

2.7 Identification of RNA modification phenotype-related DEGs

A total of 1410 BCa patients were stratified into two different RNA modification patterns in line with the preceding consensus clustering algorithm. RNA phenotype-related DEGs between Cluster 1 and Cluster 2 were determined using the empirical Bayesian method of “limma” R package [89]. DEG with $\left|\log_2 \text{fold change (FC)}\right| > 1$ and an adjusted P value < 0.001 was considered as the significance criteria.

2.8 Construction and validation of the RMS model

We further established a scoring model to assess RNA modification pattern of each BCa patient —— the signature of RNA modification “writers”, and we termed as the RMS. Initially, univariate Cox regression analysis was carried out to estimate the HR of RNA phenotype-related DEGs using “survminer” R package. Among the resulting DEGs with significantly prognostic power (P < 0.05) based on univariate Cox regression analysis, pivotal prognostic DEGs were further identified by the LASSO with L1-penalty using “glmnet” R package [90], ultimately formulating the RMS model. The LASSO method determines interpretable prediction rules that can resolve the collinearity and overfitting problem, which is applied to build models when there are plenty of correlated covariates [91]. In this algorithm, a sub-selection of RNA phenotype-related DEGs associated with BCa patients’ prognosis was identified through shrinkage of the regression coefficient and fewer parameters with a weight of nonzero ultimately remained. Thus, LASSO Cox regression reinforced the prediction accuracy of the model through diminishing the number of DEGs [92]. Subsequently, RNA phenotype-associated prognostic model was established through multiplying the regression coefficient derived from LASSO Cox regression by the expression level of each DEG. We

defined the RMS of each case in the meta-GEO using the following formula: RMS = β_{mRNA1} * $Expr_{mRNA1}$ + β_{mRNA2} * $Expr_{mRNA2}$ + ⋯⋯ + β_{mRNAn} * $Expr_{mRNAn}$, where Expr was the expression level of DEG and β was the Cox regression coefficient. Eventually, we categorized all BCa cases in the meta-GEO dataset into RMS-high and -low groups using the median risk score. To reap a uniform cutoff value to classify the cases into high and low RMS groups, a normalization for the expression values of DEGs were normalized with standard deviation (SD) = 1 and average value = 0 in the TCGA-BLCA and meta-GEO cohort. To further validate the RMS model, the risk score calculation for each patient and the stratification of patients in the TCGA-BLCA was determined according to the same formula and the identical cutoff value derived from the meta-GEO cohort, respectively.

2.9 Construction and validation of nomogram model

All statistically significant clinicopathological characteristics identified by multivariate Cox analysis were included to build the prognostic nomogram model with “rms” R package, thereby estimating survival probability of BCa individuals [81, 93]. The concordance index (C-index) and calibration curves were applied for assessing the prediction accuracy of the nomogram. The closer to 1 the C-index is, the more accurate the predictive efficiency of nomogram is [81]. The time-dependent receiver operating characteristic (ROC) curve with an area under the curve (AUC) value was formulated by “survivalROC” R package, thereby evaluating the predictive performance of the nomogram [93].

2.10 Analysis of RMS-related DEGs in pan-cancer

The online GSCALite website (http://bioinfo.life.hust.edu.cn/web/GSCALite/) was applied for exploring the mRNA expression, CNV, and pathway activity of RMS-related DEGs in pan-cancer [94].

2.11 Characterization and survival analysis of APA events between RMS-high and -low group

APA profile in BCa was downloaded from Synapse (https://www.synapse.org/, syn7888354) [42]. The DaPars algorithm (https://github.com/ZhengXia/DaPars) has been used to estimate the relative polyA site usage in 3’UTR caused by APA through the Percentage of Distal polyA site Usage Index (PDUI) that is a quantitative index to determine 3’UTR lengthening (positive index) or shortening (negative index) [43]. The Wilcoxon rank-sum test was used to compare the differences in 3’UTR between RMS-high and -low group, and we considered $P < 0.05$ and $|\Delta PDUI| = |PDUI_{RMS-high} - PDUI_{RMS-low}| > 0.1$ as statistically significant.

Univariate Cox regression analysis was performed to determine the prognostic significance of each differential APA event between RMS-high and -low group using “survival” R package. All BCa patients in the TCGA were stratified into two groups in accordance with PDUI value, and Kaplan-Meier curve with log-rank test was established to assess their survival difference.

2.12 Correlation analysis of the RMS and drug sensitivity

We acquired RNA-seq data of 18 kinds of BCa cell lines, AUC values as drug response measurements of antineoplastic drugs in BCa cell lines, and targets or pathways of drugs from Genomics of Drug Sensitivity in Cancer (GDSC, https://www.cancerrxgene.org/) [95]. Spearman correlation analysis was conducted to estimate the association between drug sensitivity and the RMS, with the cutoff values of | Spearman Correlation Rs | > 0.2 and FDR < 0.05.

2.13 Statistical analysis

Difference analysis was performed by Wilcoxon rank-sum test. Survival curve was established using Kaplan-Meier method, and log-rank test was utilized to estimate the significance of differences. Tumor and Immune System Interaction Database (TISIDB, http://cis.hku.hk/TISIDB/; up to March 15, 2021) was utilized to unravel the correlation between the abundance of various tumor-infiltrating immune cells and the expression of RNA modification “writers” genes [96]. The “pROC” R package was utilized to formulate ROC curve with corresponding AUC value, thus verifying the predictive power of the RMS model. Univariate Cox analysis was applied for calculating the HR value of RNA phenotype-associated DEGs. All significant independent prognostic factors were identified via multivariable Cox regression analysis using “survminer” R package. The Benjamini-Hochberg algorithm was used to convert P value to FDR [97]. All statistical analysis was conducted using R 3.6.2 software, and P < 0.05 were considered statistically significant.

3. Results

3.1 Genetic and transcriptional landscape of five types of RNA modification “writers” in BCa

In accordance with published articles depicting RNA modification [16, 23, 98, 99], a catalog of 34 RNA modification “writers” were enrolled into our study, including 9 m^6A modification “writers” (METTL3, METTL14, RBM15, WTAP, KIAA1429, ZC3H13, METTL16, CBLL1 and RBM15B), 2 m^6A_m modification “writers” (PCIF1 and METTL4), 5 m^1A modification “writers” (TRMT6, TRMT61A, TRMT10C, TRMT61B, RRP8), 15 APA modification enzymes (CPSF1/2/3/4, NUDT21, CPSF6/7, CSTF1/2/3, WDR33, FIP1L1, CLP1, PCF11, PABPN1), and 3 A-to-I modification enzymes (ADAR, ADARB1 and ADARB2) (**Table S1**).

To delineate genetic landscape of RNA modification “writers” in BLCA, we evaluated the frequency of non-silent somatic mutations in 34 “writers” based on mutational information of the TCGA-BLCA database. Specifically, 127 of 412 BLCA cases (30.83%) experienced mutations of RNA modification “writers”. METTL3 displayed the greatest mutation frequency (4%), followed by PCF11 (4%), KIAA1429 (3%), and WDR33 (3%). While the mutation frequency of ADARB1, METTL16 and CPSF7 was extremely low in BCa samples. Missense mutation constitutes the predominant type of mutations for each writer (Fig. 1a).

We demonstrated that BCa patients with mutant “writers” exhibited a significantly prolonged OS than those without mutation (HR = 0.53, 95% CI: 0.38–0.75, P < 0.001) (Fig. 1b), indicating that genetic

alteration of “writers” potentially exerts a functional effect towards BCa tumorigenicity. GSEA was carried out to decipher biologic themes specific for “writers” mutated (“Writers” ^{MUT}) group (N = 126) and “writers” wild-type (“Writers” ^{WT}) group (N = 285) of patients in the TCGA-BLCA. “Writers” ^{WT} group was markedly enriched in carcinogenic activation pathways, such as angiogenesis, PI3K signaling, MAPK activity, P53 signaling, Jun kinase activity, and canonical Wnt signaling pathway (Fig. 1c; **Table S2 and S3**). Hence, the mutation of “writers” is prone to trigger functional alterations with prognostic significance in BCa.

We also investigated CNV alteration frequency of these “writers” and unraveled that ADAR, ADARB2, CLP1, and CPSF7 had a relatively high frequency of CNV amplification, while ZC3H13, RBM15B and RRP8 experienced a widespread frequency of CNV deletion (Fig. 1d). To determine whether CNV plays a considerable role in the expression of RNA modification “writers” in BCa patients, we attempted to assess the mRNA level of “writers” between normal and BCa tissues in the TCGA database. As depicted in Fig. 1e to 1i, a large proportion of enzyme-associated genes displayed relatively greater mRNA expression in BCa than normal tissues, highlighting the profound function of these “writers” in the occurrence and development of BCa. Moreover, RNA modification “writers” with CNV gain (such as ADAR, CLP1, and CPSF6) were significantly up-regulated in BCa samples than normal tissues. On the contrary, the expression of “writers” genes with CNV loss (including ZC3H13 and RRP8) was significantly diminished in BCa versus normal bladder tissues. Notably, certain “writers” (such as ADARB2 and PCF11) with widespread frequency of CNV gain harbored decreased mRNA level in BCa compared to adjacent non-tumor tissues (Fig. 1d, 1g and 1h).

To further elucidate the association between CNV values and mRNA expression in BCa samples, we stratified the TCGA-BLCA cohort into three groups according to CNV values of four “writers” characterized with exceeding 5% of CNV loss in BCa tissues, including CNV gain, CNV loss and non-significant alteration of CNV. Concretely, ZC3H13, RBM15B, RRP8, and RBM15 with CNV gain exhibited dramatically enhanced mRNA level than that with CNV loss, respectively. Nevertheless, the mRNA levels of above “writers” were significantly decreased or without remarkable alteration in CNV loss group compared with those in non-tumor samples (**Figure S2a**). Thus, CNV alteration partially explains why there is differential mRNA expression between tumor and normal samples [100]. Additional parameters, such as DNA methylation and transcription factors, are also endowed with the robust capacity to orchestrate gene expression in tumorigenesis [101, 102].

3.2 Prognosis and immune characteristics of RNA modification “writers” in BCa

Pairwise correlation analysis demonstrated that not only RNA modification “writers” in the same functional category exhibited a significant correlation in expression, but also a significant correlation was presented among mRNA levels of different category of “writers”. For example, BCa samples with high expression of A-to-I “writer” gene ADAR were accompanied by increased mRNA levels of eight m^6A “writer” gene, including METTL14, RBM15, WTAP, VIRMA, ZC3H13, METTL16, CBLL1 and RBM15B, indicating a potential crosstalk between m^6A and A-to-I modification in BCa (Fig. 2a). Whether co-

expression phenomenon of these “writer” genes hints a functional correlation is a topic that motivates us to pursue further investigation. Additionally, prognosis analysis demonstrated that seven of 34 RNA modification “writers” were prognostic parameters of BCa cases in the TCGA-BLCA. Concretely, BCa patients with high METTL4 expression had a significantly longer survival time than those with low expression (HR = 0.71, 95% CI: 0.53–0.96, P = 0.0249), while those with higher KIAA1429 expression had a shorter survival time (HR = 1.35, 95% CI: 1.01–1.82, P = 0.0447) (**Figure S2b**). To further comprehensively expound the expression pattern of 34 “writers” in BCa, 1410 BCa patients from eight independent GSE sets were combined into a meta-GEO group in our study (**Table S4**).

RNA modification has recently gathered researchers’ attention because of its pertinent role in immune modulation and the TME. Thus, we reasoned the association between RNA modification “writers” and tumor immunity. As revealed in Fig. 2b **and Figure S2c**, METTL4 expression displayed a positive correlation with the subpopulation of tumor-infiltrating $CD8^+$ T cells and natural killer cells (NK cells) with anti-tumor activity while was negatively associated with the proportion of myeloid derived suppressor cells (MDSCs) with immunosuppressive effect based on the meta-GEO cohort, and this is one of reasons why METTL4 were characterized with favorable prognostic value in BCa. Additionally, BCa patients with high KIAA1429 expression were characterized with an increased proportion of macrophage and Type 17 T helper cells (Th17 cells). We also mined the GSCALite web server and found that METTL4 might play a positive role in cell cycle and DNA damage response signaling pathways in BCa; nevertheless, there was no significant association between METTL4 expression and an array of tumor-promoting signals, including PI3K/Akt, TSC/mTOR, RAS/MAPK and receptor tyrosine kinase (RTK) pathways. Inversely, KIAA1429 expression was negatively related to apoptosis, and positively associated with PI3K/Akt and RTK pathways (Fig. 2c). The IHC experiment result also verified the greater expression of KIAA1429 protein in BCa tumor samples than normal tissues (**Figure S2d**). These results further implied the carcinogenic properties of KIAA1429 in BCa.

3.3 WGCNA used for the screening of METTL4

Considering that the broad impacts of m^6A_m “writer” METTL4 on epigenetic modifications and the positive association between METTL4 and multiple immune cells in BCa samples, we further emphatically discussed the prognostic significance of METTL4 in BCa. Initially, a total of 5657 prognosis-associated genes were extracted in 411 BCa patients, among which 3497 genes were associated with favorable prognosis (HR < 1, P < 0.05) and 2160 genes were related to unfavorable prognosis (HR > 1, P < 0.05). To select pivotal hub genes associated with BCa progression, above 5657 prognosis-associated genes were applied to cluster analysis by the “WGCNA” R package. On the basis of the standard scale-free network distribution, we carefully set the soft threshold power value as 7 to formulate a hierarchical clustering tree (dendrogram) of 5657 genes (Fig. 2d). According to the dynamic tree cut algorithm, the least gene number of each module and the minimum cut height was 50 and 0.25, respectively. The correlation of characteristic genes in integrated modules was over 0.9. We identified six co-expression modules containing all genes based on their degree of connectivity. The gray section represented background genes that did not belong to any modules (Fig. 2e). We ultimately assessed the correlation

between MEs and clinical traits, including TNM stage, histological grade and survival status. Specifically, the brown module was characterized with the strongest negative correlation with survival status (r = -0.82, P < 0.0001), which was considered as the most significant module to the prognosis of BCa (Fig. 3a). There were four RNA modification “writers” in the brown module, of which MM value and the absolute value of GS of METTL4 ranked first (P < 0.0001) (Fig. 3b). Thus, METTL4 can be defined as one hub gene significantly related to survival status and BCa prognosis in the brown module.

GSEA analysis further revealed that six immune-associated pathways, such as regulation of receptor binding, Th17 type immune response, leukocyte adhesion to vascular endothelial cell, B cell differentiation, and negative regulation of IL-6 production and response to IFN-γ, were significantly enriched in high METTL4-expressing group (Fig. 3c **and Table S5**). Eventually, we also investigated whether METTL4 expression could predict patients’ response to ICB treatment. Specifically, 348 patients in IMvigor210 cohort displayed varying degrees of clinical benefits from anti-PD-L1 treatment, including complete response (CR), partial response (PR), stable disease (SD), and progressive disease (PD). We demonstrated that patients with high METTL4 expression had a notably prolonged OS and prominently therapeutic advantage in IMvigor210 cohort (HR = 0.72, 95% CI = 0.54–0.96, P = 0.02) (Fig. 3d). Similar tendency was also identified in Snyder UC cohort (HR = 0.48, 95% CI = 0.18–0.79, P = 0.014) (Fig. 3e). The hypotheses regarding METTL4 expression as favorable prognostic indicator affected by its antitumor property came to light from the above bioinformatic approaches. Future mechanistic investigations of biological functions of METTL4 in BCa are required.

3.4 Immune landscape of RNA modification-associated patterns in BCa

On the basis of the expression profiles of 34 RNA modification “writers” in the meta-GEO cohort, we conducted unsupervised consensus clustering to stratify BCa patients with qualitatively varying RNA modification patterns into two distinct clusters, eventually including 1063 cases in Cluster 1 and 347 cases in Cluster 2, respectively (Fig. 4a **and Figure S3a**). Specifically, Cluster 1 had significantly increased presence of RBM15, WTAP, KIAA1429, TRMT6, TRMT61B, CPSF3, CPSF4, WDR33 and ADARB1, while Cluster 2 was characterized with elevated level of METTL14, ZC3H13, METTL16, PCIF1, METTL4, RRP8, CPSF1 and ADARB2 (Fig. 4b **and Figure S3b**). Furthermore, based on above-identified clusters, BCa patients in Cluster 1 and Cluster 2 were visibly separated into two discrete groups using three dimensional PCA, emphasizing that BCa cases are well stratified in line with the mRNA levels of 34 RNA modification “writers” (Fig. 4c). Survival analysis for two primary RNA modification subtypes demonstrated that compared with Cluster 1 modification pattern, Cluster 2 pattern was linked to significantly prolonged survival (HR = 0.63, 95% CI = 0.43–0.91, P = 0.013) (Fig. 4d). We further conducted GSVA to investigate the biological behaviors of above different RNA modification patterns. The carcinogenic activation pathways, including the epidermal growth factor activated receptor activity, TLR-2 signaling pathway, chemokine CXCL2 production and cell adhesion, were enriched relative to Cluster 1, indicating an inflammation activation and tumorigenesis status in Cluster 1. While Cluster 2 represented a metabolic or biosynthetic activation phenotype, prominently enriched in pathways related to the cyclic

nucleotide catabolic process, CAMP-dependent protein kinase activity and DNA replication (Fig. 4e **and Table S6**).

We also unraveled the discrepancies concerning the compositions of tumor-infiltrating immune cells between two RNA modification clusters. Significant difference in immune cell fractions in two primary patterns were summarized in **Table S7 and S8**. As revealed in Fig. 4f **and Figure S3c**, Cluster 1 was characterized with an increased proportion of MDSCs with formidable immunosuppressive property ($P < 0.0001$) and Th17 cells ($P < 0.0001$). Conversely, cases in Cluster 2 exhibited prominent infiltration of activated $CD8^+$ T cells with pronounced antitumor activity ($P < 0.001$), effector memory $CD4^+$ T cells ($P < 0.0001$), and central memory $CD8^+$ T cells ($P = 0.032$). Consistently, compared with cases in Cluster 2, those in Cluster 1 had significantly increased levels of MDSC marker genes (including STAT2, S100A9, CXCL2, CSF1, PTGS2, TREM1, CEBPB) while significant down-regulation of activated $CD8^+$ T cell marker genes (such as CD8A, IFN-γ, IL-13, and FASLG) (Fig. 4g). In summary, RNA modification patterns exert an effect on the proportions of infiltration by specific immune cell types while fail to change the types of infiltrating immune cells.

3.5 Establishment of the RMS model and its clinical significance in BCa

We further determined 632 RNA modification phenotype-associated DEGs between Cluster 1 and Cluster 2. The biological processes with significant enrichment associated with these DEGs were enriched in purine nucleotide metabolic process, methylation, DNA replication, and cell cycle G1/S phase transition, all of which were closely related to RNA processing (**Table S9 and Figure S4a**). In consideration of the heterogeneity and complexity of RNA modification, we attempted to establish a risk score system named the RMS (RNA Modification “Writers” Score). Firstly, we confirmed that 119 of 632 DEGs was significantly correlated with OS through univariate Cox regression analysis (**Table S10**). To reveal potential DEGs with the optimal prognostic performance, we utilized LASSO Cox analysis, and 14 DEGs were incorporated into our subsequent analysis. Notably, IFNLR1 (HR = 1.95, 95% CI: 1.47–2.58, $P < 0.0001$) was identified as a crucial RNA phenotype-associated and prognosis-related DEGs with the largest beta value (0.206), implying its optimal prognostic efficiency in BCa patients (**Table S11; Figure S4b and S4c**). Furthermore, we performed normalization of the expression levels of 14 DEGs in the TCGA and meta-GEO cohort with average value = 0 and SD = 1, thus acquiring a uniform cutoff value as stratified standard. Then, we quantified the RNA modification status of each BCa patient by weighting the normalized mRNA level of each DEG to the regression coefficient. The concrete formula was the following: $RMS = 0.2062 * Expr_{IFNLR1} + 0.1822 * Expr_{PCDHB11} + (-0.1428) * Expr_{TIMM21} + \ldots\ldots + 0.0057 * Expr_{CRELD1} + 0.0028 * Expr_{FOXG1}$. Ultimately, we calculated the RMS for each BCa case in the meta-GEO and stratified all cases into RMS-high and -low cohorts based on the median value (3.344) (**Table S12**).

As showed in Fig. 5a, the RMS classified BCa cases with high or low risk score into two discrete sections, highlighting that the RMS distribution of BCa cases in the low-risk group was greatly different from those with high risk score. There was a high degree of consistency among the risk score distribution, the

heatmap of 14 prognostic DEGs' expression and survival status of BCa case in the meta-GEO cohort (Fig. 5b). Notably, the cutoff point (3.344) also served as a classification indicator in the TCGA-BLCA cohort. Kaplan-Meier curve revealed that high RMS was significantly correlated with more unfavorable clinical outcome of BCa cases in the meta-GEO (HR = 3.00, 95% CI: 2.19–4.12, P = $1.06e^{-11}$) (Fig. 5c) and TCGA-BLCA cohort (HR = 1.53, 95% CI: 1.13–2.09, P = 0.006) (Fig. 5d). Additionally, patients with high RMS had a shorter disease-specific survival (DSS) than their RMS-low counterparts in GSE32894 (HR = 18.3, 95% CI: 4.30–77.6, P < 0.001) (**Figure S4d**). In GSE31684 dataset with recurrence data, the RMS was significantly negatively associated with recurrence-free survival (RFS) (HR = 2.02, 95% CI: 1.06–3.88, P = 0.033) (**Figure S4e**). We also investigated the correlation between the RMS and cluster classifier to evaluate the RMS model's accuracy. As revealed in Fig. 5e, the RMS of BCa samples in Cluster 1 was significantly higher than that of cases in Cluster 2 (P = 0.025). We found that 579 out of 742 (78.03%) samples with high RMS were overlapped with the samples in Cluster 1, and 184 out of 668 (27.54%) cases in RMS-low group overlapped with the individuals in Cluster 2 (**Figure S4f and S4g**). Therefore, there is a high degree of coincidence among three computational methods of classification.

Univariate Cox analysis indicated that certain clinical variables, including age, M classification, N classification, T classification, TNM stage, and RMS exhibited an impact on the survival of BCa patients (Fig. 5f). Above significant parameters were included into subsequent multivariate Cox regression analysis. The corresponding findings revealed that age > 65 years (HR = 1.87, 95% CI: 1.33–2.64, P = 0.00032), advanced N classification (HR = 1.62, 95% CI: 1.17–2.25, P = 0.00403), and high RMS (HR = 1.61, 95% CI: 1.17–2.24, P = 0.00388) remained adverse and independent prognostic factor in BCa (Fig. 5f). These findings imply that the RMS model is independent of conventional clinical variables and can predict the survival of BCa with comparatively satisfactory performance. Additionally, based on WGCNA method, the green module was most significantly positively correlated with survival status of BCa (r = 0.76, P < 0.0001) (Fig. 3A), and IFNLR1 was one of the most significant hub genes in the green module (Fig. 5g), indicating that IFNLR1 was one of the DEGs that was the most significantly correlated with prognosis than other 13 DEGs in the RMS model. Additionally, we performed IHC of BCa samples and matched bladder tissues from 84 cases with primary BCa to further investigate IFNLR1 protein expression level in BCa. IFNLR1 protein was significantly increased in BCa tissues compared with adjacent normal bladder samples (Fig. 5h).

To confer physicians with a visualized approach to predict the long-term survival of BCa patients, the nomogram model encompassing the RMS signature and significant clinical risk factors identified by multivariate Cox analysis was formulated. As illustrated in Fig. 6a, N classification made the greatest contributions to risk points, followed by age and the RMS model. The C-index of the nomogram was 0.745 (95% CI: 0.697–0.798) under 1000 bootstrap replication. The calibration curves for the OS probability of 1-, 3-, and 5-year in BCa cases demonstrated a good agreement between nomogram prediction and practical observation (Fig. 6b). The time-ROC curves were established to compare the predictive efficiency of this nomogram with that of N classification, age and the RMS. For the ROC curve of 1-year survival, the AUC of nomogram (0.671) was higher than that of age (0.622), N classification

(0.582), and the RMS (0.54) (Fig. 6c). The nomogram to predict 3-year OS obtained the optimal AUC of 0.675, followed by N classification (0.603), age (0.588), and the RMS (0.558) (Fig. 6d). The AUC for the nomogram, N classification, age and the RMS to predict 5-year survival were 0.706, 0.625, 0.584, and 0.601, respectively (Fig. 6e). The decision curve analysis (DCA) of the nomogram was characterized with the optimal net benefits, followed by N classification, age, and the RMS (Fig. 6f). In sum, the nomogram incorporating N classification, age and the RMS exhibits a relatively satisfactory predictive performance for the long-term survival of BCa patients.

3.6 Molecular subtypes and functional annotation associated with the RMS in BCa

We further illustrated the functional characteristics of the RMS signature through analyzing the association between the RMS model and known biological processes-associated gene sets identified by MSigDB [87], emphasizing that high RMS was significantly associated with stromal activation status and cancer progression-associated pathways, such as inflammatory response, NF-KB-mediated TNF-a, epithelial-mesenchymal transition (EMT), angiogenesis, IL-6/JAK/STAT3 signaling (Fig. 7a **and Figure S4h)**.

Based on a comprehensive molecular subtypes landscape of UC established by Sjödahl et al.'s study [70], UC cases were classified into five molecular subtypes, including urobasal A (MS1 subdivided into MS1a and MS1b), genomically unstable (MS2a subdivided into MS2a1 and MS2a2), urobasal B (MS2b2.1), squamous cell carcinoma (SCC)-like (MS2b2.2), and one highly infiltrated by nontumor cells (MS2b1). Notably, above molecular subtypes differed in survival patterns in which urobasal A exhibited favorable prognosis, genomically unstable and the infiltrated group were with moderate prognosis, and the urobasal B and the SCC-like were characterized with the shortest survival [70]. We compared the difference of the RMS among above five molecular subtypes through analyzing data downloaded from GSE32894. The SCC-like subtype showed the highest RMS, followed by the urobasal B, genomically unstable, the infiltrated subgroup and urobasal A (Fig. 7b). Additionally, there was a significant discrepancy in the distribution of molecular subtypes between RMS-high and -low group. The urobasal A subtypes was primarily clustered in RMS-low group, conversely, the SCC-like and the infiltrated subtype were markedly concentrated on RMS-high group (Fig. 7c).

To further decipher potential biological processes associated with different molecular subtypes of BCa patients in GSE32894, GSVA was performed implying that tumorigenesis- associated biological processes were significantly enriched in the SCC-like and the urobasal B subtype, including WNT, NOTCH, angiogenesis, and IL2-STAT5 signaling pathways. In contrast, the biological pathways activated in the urobasal A subtype were significantly correlated with the heme metabolism, protein secretion and peroxisome (Fig. 7d). Consistently, the SCC-like and the urobasal B-related signaling pathways were prevailingly enriched in RMS-high cases, while the enrichment score of urobasal A-related biological processes were markedly clustered in RMS-low group (**Figure S4h**). BCa patients in the urobasal B and the SCC-like subtype were prone to be diagnosed at more advanced stage compared with those in the

urobasal A subtype (Fig. 7e), which was also significantly correlated with diminished OS (HR = 12.3, 95% CI: 1.36–111, P = 0.026 for the urobasal B subtype) (Fig. 7f). Previous results in our report demonstrated that the RMS positively correlated with BCa patients' degree of malignancy. Thus, high RMS roughly corresponding to the urobasal B and the SCC-like subtype indicates unsatisfactory prognosis, which is potentially partly ascribed to the activation of EMT, WNT, angiogenesis, and additional signaling pathways mediating BCa tumorigenicity and tumor metastasis.

3.7 Pan-cancer analysis of RMS model-associated genes

Initially, we explored the correlation between CNV and mRNA expression in 14 RMS model-associated genes in 33 kinds of tumors and revealed that CHMP7 expression was significantly modulated by CNV in almost all cancers, followed by SEPHS1 and AASDHPPT (**Figure S5a**). Specifically, a majority of RMS model-associated genes was characterized with heterozygous amplification of CNV in adenoid cystic carcinoma, while homozygous amplification was prone to occur in OV, esophageal cancer, and unconditioned stimulus (**Figure S5b**). Thus, the findings highlight that the CNV of RMS model-associated genes is various among different tumors and it is essential to investigate the source of the heterogeneity. Furthermore, we explored the difference in mRNA expression between tumor and normal sample and revealed that the fold difference in the expression of RMS model-associated genes was the greatest in LUSC. Concretely, GDPD5 and IL28RA were significantly downregulated in BRCA than normal samples, while ROMO1 was overexpressed in BRCA samples (**Figure S5c**). Additionally, pathway analysis demonstrated that RMS model-associated genes principally triggered cell cycle and EMT pathway while exerts an inhibitory effect on apoptosis and RAS/MAPK pathway (**Figure S5d**). Therefore, our RMS model genes potentially plays a crucial role in malignant progression of tumors.

3.8 Difference in post-transcriptional events between RMS-high and -low groups in BCa

To elucidate the functional effect of RNA modification "writers" on post-transcriptional characteristics of BCa patients, we investigated APA events of each gene in the TCGA-BLCA. Initially, we analyzed APA alterations between 246 BCa cases with high or low RMS and determined the prognostic significance of transcripts with significant 3'UTR alterations. A total of 11598 APA events remained for differential analysis, and there were 503 genes with significantly lengthened 3'UTR (ΔPDUI > 0.1) and 96 transcripts with markedly shortening 3'UTR (ΔPDUI < 0.1) in RMS-high group, respectively (P < 0.05) (Fig. 8a **and Table S13**), and shortening APA events in RMS-high group were characteristic with worse OS based on univariate Cox regression analysis (Fig. 8b **and Table S14**), thus indicating that usage of a PAS may exacerbate BLCA malignancy. Specifically, the transcripts of *CCNO* (ΔPDUI = -0.16, P = 0.003) and *PAOX* (ΔPDUI = -0.15, P = 0.03) both underwent statistically significant 3'UTR shortening in patients with high RMS, which was associated with worse survival in BLCA (HR = 1.92, 95% CI: 1.30–2.86, P = 0.001 for *CCNO*; HR = 1.52, 95% CI: 1.02–2.22, P = 0.039 for *PAOX*) (Fig. 8c). A report have demonstrated that *CCNO* is overexpressed in cervical squamous cell carcinoma (CSCC) and RACK1/ miR-302b/c/d-3p-mediated CCNO inhibition can dampen the progression of CSCC [103]. Suppression of *PAOX* is sufficient to widen the therapeutic index of cytotoxic drugs and overwhelm DNp73-mediated chemoresistance in cancers

[104]. Thus, we speculate that shortening 3'UTR of *CCNO* and *PAOX* in BLCA samples with high RMS potentially results in loss of several RNA regulatory elements, such as miRNA binding sites, thus enabling the upregulation of oncogenes expression and the progression of BLCA.

3.9 Potential role of the RMS in antitumor chemotherapy and antibody-drug conjugates (ADC) therapy

To further assess the relationship between the RMS and drug response of BCa cell lines, we determined 34 significantly correlated pairs between the RMS and drug response in the GDSC database based on Spearman correlation analysis [95]. Specifically, there was significant correlation between drug sensitivity and the RMS in 8 pairs, including EGFR inhibitor HG-5-88-01 (Rs = -0.804, P = 0.005), CSF1R inhibitor GW-2580 (Rs = -0.43, P = 0.016), and AR inhibitor Bicalutamide (Rs = -0.383, P < 0.0001). Conversely, 26 pairs displayed drug resistance significantly related to the RMS, including JNK1 inhibitor ZG-10 (Rs = 0.867, P < 0.0001) and CDK9 inhibitor THZ-2-49 (Rs = 0.625, P < 0.0001) (Fig. 9a **and Table S15**). Additionally, we also explored the potential signaling pathways of drug-targeted genes. As revealed in Fig. 9b, drugs whose sensitivity was linked to high RMS primarily targeted hormone-related, ADCK4, and EGFR signaling pathways, while drugs whose resistance was related to high RMS mostly targeted DNA replication, cell cycle and PI3K/MTOR signaling pathways. Thus, above findings indicate that RNA modification patterns are related to drug response of tumors. The RMS potentially develops into a novel biomarker to confer a reference for appropriate clinically interventional strategies.

ADCs are novel targeted agents that concatenate a cytotoxic drug (also known as cytotoxic payload or warhead) by a linker to a monoclonal antibody (mAb) which can specifically reach target antigens expressed on cancer cellular surface and deliver a potent cytotoxic payload to the tumor location, ultimately strengthening the chemotherapeutic efficacy and minimizing toxicity to normal tissue. The target antigen should be abundantly expressed on tumor cells while is not expressed or at a low level in normal tissues in an ideal setting, thus lowering off-target toxicity [105]. Currently, certain ADCs have been approved by the US Food and Drug Administration (FDA) for the cancer therapy (**Table S16**) [106–113]. Two target antigens (ERBB2 and TROP2) were lineage-specific markers of two out of above approved ADCs——Trastuzumab deruxtecan, and Sacituzumab govitecan, which have consistently high expression across the BCa tumor population than normal samples in the TCGA-BLCA (Fig. 9c). We further evaluated the differences in the expression of seven target antigen molecules of ADC in RMS-low and -high groups. The target antigens, including ERBB2 and TROP2, were preferential expression on RMS-high BCa samples with a relative low expression on RMS-low subgroup (Fig. 9c). Together, above findings implied that RNA modification patterns are potentially associated with ADC sensitivity.

3.10 Predictive value of the RMS in immunotherapeutic efficacy

Immunotherapies of blocking T-cell inhibitory molecules PD-L1 and PD-1 have undoubtedly emerged a significant breakthrough in anticancer intervention. Meanwhile, it is urgent for us to make judgment about

which subset of patients can benefit most from immunotherapies [114]. Therefore, we investigated the predictive power of the RMS for patients' response to ICB therapy based on two immunotherapy cohorts. Patients with low RMS exhibited significantly prolonged OS than those with high RMS in IMvigor210 cohort (HR = 0.76, 95% CI: 0.58–0.99, P = 0.040) (Fig. 10a). For IMvigor210 cohort, Chi-squared test demonstrated that compared with RMS-high group, RMS-low group was endowed with markedly increased proportion of the sum of CR and PR patients while significantly diminished the sum of PD and SD cases (P = 0.037) (Fig. 10b). Likewise, CR patients were characterized with the lowest RMS compared with their counterparts with other types of response (Fig. 10c). Significant therapeutic advantage and strengthened clinical response to anti-MAGE-A3 immunotherapy in patients with low RMS were also confirmed in Montoya melanoma cohort (Fig. 10d and 10e). Additionally, we also validated the predictive performance of the RMS in anti-MAGE-A3 immunotherapy, with a satisfactory AUC value of 0.712 (Fig. 10f). Collectively, cases with lower RMS are more possibly to reap better prognosis and enhanced clinical benefit from ICB therapy.

Accumulated evidence has emphasized that patients with elevated TMB, higher neoantigen burden, certain DNA repair mutations, mismatch repair deficiency, and higher PD-L1 expression level are correlated with improved objective response, durable clinical benefit, and prolonged long-term survival when receiving ICB therapy [115, 116]. Based on tumor-associated immune phenotypes depicted in IMvigor210 cohort, patients with low RMS were characterized with significantly increased PD-L1 level (Fig. 11a). Similarly, cases in RMS-low group had significantly strengthened TMB and neoantigen burden than those with high RMS (Fig. 11b and 11c), indicating a potential response to ICB. Patients with the combination of low RMS and high TMB/neoantigen burden displayed the optimal survival advantage (HR = 0.51, 95% CI: 0.33–0.79, P = 0.003 for Low RMS with high TMB; HR = 0.48, 95% CI: 0.31–0.76, P = 0.002 for Low RMS with high neoantigen burden) (Fig. 11d and 11e). We further explored the difference in the RMS among three phenotypes, including "immune inflamed", "immune excluded", and "immune desert" [117]. As illustrated in Fig. 11f, patients with an immune-inflamed phenotype exhibited the lowest RMS compared with the other two phenotypes. Above findings partly explain why immunotherapy is prone to exert intensive antitumor effect in the low RMS subset. Our aforementioned results also demonstrated that MDSC which is recognized to mediate immune tolerance in the TME was significantly activated in RMS-high group, indicating that RMS-high tumors potentially represent "cold tumors" with resistance to immunotherapy. Furthermore, AUC value evaluating the capacity of the RMS model, TMB, TNB and PD-L1 to differentiate responders from non-responders was 0.677 (95% CI = 0.589–0.765), 0.652 (95% CI = 0.549–0.755), 0.690 (95% CI = 0.595–0.785), and 0.625 (95% CI = 0.517–0.733), respectively. The results also illustrated that the RMS in combination with TMB, TNB and PD-L1 had the optimal predictive power, with the highest AUC of 0.828 (95% CI = 0.714–0.941), followed by TMB combined with TNB and PD-L1 (AUC = 0.797, 95% CI = 0.678–0.916), the RMS combined with TNB (AUC = 0.765, 95% CI = 0.671–0.859), the RMS combined with TMB (AUC = 0.742, 95% CI = 0.641–0.843), and the RMS combined with PD-L1 (AUC = 0.708, 95% CI = 0.595–0.822) (Fig. 11g). Briefly, these results may introduce the novel piece to the atlas of RNA modification patterns' influence on the efficacy of immunotherapy.

4. Discussion

4.1 PPPM/3PM concept in the current study

The building blocks of RNA are canonically confined to four bases, nevertheless, RNA modifications can tremendously expand the chemical diversity of RNA. It is therefore not surprising that RNA modifications have attracted much attention recently owing to their sophisticated and widespread impacts on inflammation, innate immunity, antitumor activity, and the response to immunotherapy through the cross-talk among multifarious “writers”. With the exception of certain studies centralized a single type of RNA modification “writer”, there has been no literature so far of a comprehensive elucidation in the multifaceted association and effects of diverse types of “writers” on malignancy [118, 119]. Therefore, in our report, we unveiled the global profiling of RNA modification patterns and its impact on prognostic characteristics and immune landscape in the TME of BCa and further combined the RNA modifications-related model and additional routine clinicopathological indicators to effectively predict the clinical outcome and immunotherapy effectiveness, which potentially opens up a new dimension for the PPPM/3PM development of BCa.

4.2 The role of RNA modification “writers” in the prognosis and tumor immune microenvironment (TME)

The “writers” of RNA modification exerts momentous impacts on normal growth and their mutation or disharmony is related to both genetic disorders and multiple malignancies [120]. Herein, we described the mutation landscape of 34 “writers” and its prognostic role in BCa for the first time. We found that m^6A “writers” METTL3 and KIAA1429 and APA enzymes PCF11 were more predisposed to mutation than additional “writers” in BCa, while mutations of the “writers” CPSF1, ADARB2 and KIAA1429 were proved to be more frequent in hepatocellular carcinoma (HCC) and the mutation frequency of the “writers” ZC3H13, PCF11 and KIAA1429 was the highest in colorectal cancer (CRC) [121, 122]. We also observed that mutations of 34 “writers” genes were correlated with worse OS of BCa patients, making it clear that total diminished level of RNA modification is endowed with a crucial role in BCa development. Similarly, a shorter OS in clear cell renal carcinoma (ccRCC) patients with “writers” genes loss of function was revealed [121]. The carcinogenic activation pathways were significantly enriched in HCC cases with the “writers” mutation, indicating the relationship between the mutant status of “writers” and worse outcomes of HCC patients [122]. Intriguingly, CRC cases with mutant “writers” had poorer prognosis compared with those without mutations [123]. Thus, the discrepancies of mutant status of “writers” and its associated prognostic effects between different tumor types gave us a clue that the modulation of RNA modification in cellular level was sophisticated, and more researches concentrating on the “writers” are required to further illustrate the regulatory mechanism of RNA modification in BCa.

We specifically summarized global alterations of m^6A, m^6A_m, m^1A, APA, and A-to-I RNA editing enzymes at transcriptional and genetic levels and their mutual correlation in BCa. Specifically, m^6A “writer” KIAA1429 was the third most common mutant gene and had relatively prevalent CNV gains, with a

negative association with the prognosis of BCa patients, indicating the potential function of KIAA1429 in promoting carcinogenesis and metastasis. Prior studies have confirmed significant overexpression of KIAA1429 in multifarious human cancers, including hepatocellular carcinoma (HCC) [118], breast cancer [124], non-small cell lung cancer (NSCLC) [125], gastric cancer [126], and osteosarcoma [127], which was positively correlated with malignant biological properties while linked to significantly diminished OS of above tumors. Mechanistically, KIAA1429-mediated m6A methylation on the 3'UTR of GATA3 pre-mRNA elicits the separation of HuR and the resulting degradation and downregulation of GATA3, which triggers HCC development [118]. Furthermore, KIAA1429 is sufficient to enhance the expression of CDK1 by an m^6A-independent manner and further accelerates breast cancer progression [124]. KIAA1429 favors the mRNA stability of HOXA1 via targeting its 3'UTR to confer NSCLC on gefitinib resistance, suggesting the role of KIAA1429 as potential therapeutic target in NSCLC [125]. On the contrary, m^6A_m enzyme METTL4 and APA "writer" CSTF3 were positively correlated with the survival of BCa patients and an evident enhancement in T lymphocyte infiltration, emphasizing that a wide variety of post-transcriptional modulation sets the stage for anti-tumor effects. Collectively, these findings unveil a diverse heterogeneity of RNA modification, highlighting the significance of a comprehensive evaluation of RNA modification patterns and potentiating our understanding of epigenetic modulation on numerous aspects of host pathophysiology.

4.3 The role of distinct RNA modification patterns in the prognosis and tumor immune microenvironment (TME)

In addition to elucidating the specific role of individual RNA modification "writer" in the prognosis and immunity of BCa, we also investigated the clustering result of 34 RNA modification "writers". Two distinct RNA modification patterns (Cluster 1 and Cluster 2) were identified based on 34 RNA modification enzymes. We confirmed that MDSCs and Th17 cells were accumulated in Cluster 1 cases that was characterized with poor survival and low response rate to immunotherapy. MDSCs are a cluster of pivotal immunosuppressive cells in the TME, which are endowed with the capacity to impede T cell, NK cell and B cell functions partly through stimulating the expression of ARG1, indoleamine 2, 3-dioxygenase and inducible nitric oxide synthase [128]. MDSCs also interact with tumor cell and foster its stemness characteristics, thereby maintaining a malignant phenotype of tumors [129]. MDSCs secrete diversiform chemokine receptors that are implicated in their recruitment to the TME, such as CXCR4 or CXCR2, as revealed in BCa patients [130, 131]. Therefore, blocking the recruitment of MDSCs to the TME or depleting MDSCs in the tumor is a potentially promising strategy. Previously reports have demonstrated that patients with tumor who have high levels of circulating MDSCs exhibit an undesirable response rate to immunotherapy [129]. Intriguingly, a chemical agonist LXR-mediated the activation of ApoE secretion devastates MDSC survival by facilitating the binding of ApoE to its receptor LRP8, resulting in a fortified anti-tumor response [132]. A phase I clinical trial in BCa patients, is currently testing a LXR agonist (RGX-104) as a single agent or combined with nivolumab to strengthen the anti-tumor activity and the response to anti-PD-1 therapy [129]. Pathologically, Th17 response participates in certain inflammatory events, autoimmune and allergic diseases. Th17 cells have been demonstrated in increased levels in certain

tumors, it remains controversial whether IL-17 facilitates or suppresses tumor progression. Specifically, IL-17-induced the generation of IL-6 activates oncogenic STAT3 and subsequently accelerates the expression of pro-survival and angiogenic genes, resulting in the development of BCa [133].

4.4 The RNA modifications-related signature as biomarker in the context of PPPM/3PM in BCa

We then formulated a scoring model, RMS, to evaluate the efficacy of RNA modification “writers” in each case. RMS-high group was related to worse prognosis, which was partly attributed to significant activation of EMT, Notch, IL-2/STAT5, IL-6/JAK/STAT3, angiogenesis signaling pathways, which was instrumental in tumor invasion. The biological process of EMT involves epithelial cells assuming a mesenchymal phenotype, with reinforced capability for invasion and metastasis to accelerate malignant progression of BCa [134]. In studies encompassing a wide spectrum of malignancies, including prostate cancer, breast cancer, and multiple myeloma, there is adamant evidence holding a crucial effect of Jagged-mediated Notch signaling on tumor metastasis. Notch activation drives FOXC2-dependent metastasis in PTEN-null prostate cancer mice [135, 136]. A paracrine loop composed of TGF-β and Jagged-mediated Notch activation also facilitates osteolytic bone metastasis in breast cancer [137]. Activation of IL-2/STAT5 signaling converged on an enhancer (CNS0) potentiates the generation and accumulation of IL-2 dependent thymic Treg cell lineage, potentially dampening host immune responsiveness [138]. In the pathogenesis of cancer, increased IL-6 directly on stimulate cells in the TME to upregulate STAT3 target genes, subsequently driving the expression of proliferation-promoting proteins (such as cyclin D1), survival-associated molecules (such as BCL2-like protein 1), angiogenic factors (such as VEGF), invasiveness and metastasis-related proteins (such as matrix metalloproteinases) and immunosuppressive molecules (such as IL-10 and TGF-β) [139].

Eventually, considering the remarkable effect of RNA modification patterns on immune infiltration in the TME, we showed enormous interest in the capacity of the RMS to predict the potential therapeutic effects of ICB therapy. Our findings highlight that the RMS was a potent predictor to assess the clinical outcome of distinct immunotherapy regimens (anti-PD1/L1 or anti-MAGE-3), which was validated in two UC immunotherapy cohort and two melanoma immunotherapy cohorts. The RMS combined with TMB could differentiate non-responders who underwent immunotherapy from responders with a more robust capability and a remarkably increased accuracy. Thus, our results allow the development of personalized cancer immunotherapy and advance our capacity to exploit an additional approach through which the response rate of immunotherapy can be enhanced.

4.5 Strength and limitations

RNA modifications are emerging as a novel frontier research hotspot, which is closely related to various tumor cellular processes and oncogenesis, and exerts comprehensive therapeutic implications in cancer [140]. Our study was the first link between five forms of RNA adenosine modifications (including m6A, m6Am, m1A, APA, and A-to-I editing) and the prognostic characterization and immunologic landscape in BCa. We proposed two RNA modification patterns which differed with respect to TME cell infiltrating

characteristics and further demonstrated the RNA modifications-related model as an independent prognostic predictor to stratify BCa individuals into high- and low-risk groups for patient stratification, prognostic evaluation, and personalized therapy toward PPPM/3PM in BCa. Additionally, we comprehensively analyzed the correlation between the RMS signature and immune landscape, molecular subtypes, post transcriptional modulation, drug sensitivity and immunotherapeutic efficacy of BCa. Also, WGCNA-based analysis determined the most weighted prognostic markers (METTL4 and IFNLR1) and the expression levels of above markers were analyzed in human tissue samples by IHC, thus guaranteeing the dependability of the results in this report. Despite its promising results, several limitations should be mentioned in our study. Firstly, in spite of the inclusion of 34 well-recognized RNA modification “writers” in our report based on literature search, additional novel identified “writers” should be incorporated for integral analysis, thus optimizing the accuracy of RNA modification patterns. Secondly, we merely utilized a median cutoff of the RMS based on the meta-GEO cohort to stratify BCa patients. The results need to be validated in a prospective cohort of patients treated with immunotherapy, thus more comprehensively defining the cutoff value to be used. Furthermore, considering the primary clinical significance of distinct tumor regions, it is necessary to systematically assess immune characteristics in the core of the tumor and at the invasive margin. Because not all cases with low RMS exhibit enduring and effective response to immunotherapy, other clinicopathological parameters should be included into the model to improve predictive performance.

5. Conclusions And Expert Recommendations In The Framework Of 3p Medicine

In summary, our profound and comprehensive analysis of five forms of RNA modification “writers” highlighted an extensive modulatory mechanism by which they exert effects on TME and their correlation with BCa prognosis. We determined two distinct RNA modification-associated subtypes in BCa and constructed an individual RNA modification “writers” profile scoring system that unraveled the interplay and regulatory roles of the “writers” in BCa prognosis, molecular subtypes and post-transcriptional events and depicted their predictive performance in chemotherapy, ADC therapy and immunotherapy. Our study emphasizes the pivotal clinical significance of the interaction among RNA modifications and advances our capacity to guide more effective and personalized immunotherapy for BCa, which conforms to the aim of early prediction, targeted prevention, and patient-oriented personalized medical care supported by the PPPM/3PM [141].

We strongly recommend to emphasize and popularize the vital scientific merits of pathology-specific “writers” of RNA modifications in BCa, enhance the exploration of the RNA modifications “writers” in integration with clinicopathological parameters in BCa, and facilitating the early clinical translation and optimization of RNA modifications-associated signature in the framework of PPPM/3PM in BCa. Thus, we propound the following three points: RNA modification machinery is the momentous mechanism to modulate the post-transcriptional alterations and closely linked to a variety of tumors. Firstly, the comprehensive analysis of the aberrant expression profiles of the RNA modifications regulator system

and clinicopathological indicators conferrs a scientific strategy to formulate a pathology-specific RNA modifications “writers” gene signature, which will be conducive to the optimization of BCa management in the framework of PPPM/3PM practice. Our report proposed an RNA modifications-related signature with significant association with clinicopathologic features and unsatisfactory prognosis. It can be potentially developed into an effective biomarker for patient stratification, individualized prognostic diagnosis and targeted therapy for BCa patients in the practice of PPPM/3PM. Notably, sequencing analysis for RNA modifications-related regulator genes is not confined to tumor samples acquired via intraoperative resection and puncture biopsy. For urologic neoplasms, tumor cells shed in urine confers a novel concept for the study of RNA modifications-related regulator genes in BCa, which is endowed with the advantages of non-invasive and high patient compliance. Additionally, the importance of post-transcriptional modification for the diversity of the structure and function of RNA is self-evident. To comprehensively clarify the molecular mechanisms and biological effects of the RNA modifications regulator genes on BCa, the large-scale integration of proteomics data and other multi-omics data and the identification of “writers”-targeted RNA molecules and modification sites by RNA sequencing and RNA immunoprecipitation will elevate our understanding in the pathogenesis of BCa. Furthermore, it is a promising area to explore RNA modifications machinery-based therapeutic targets and drugs for BCa, especially researches on the abnormal regulators of RNA modifications might result in more precise and reliable biomarkers and novel effective therapeutic targets/drugs for PPPM/3PM practice in BCa.

Abbreviations

PPPM/3PM: Predictive preventive personalized medicine; m^6A: N^6-methyladenosine; m^6A_m: N^6,2'-O-dimethyladenosine; m^1A: N^1-methyladenosine; APA: alternative polyadenylation; A-to-I: adenosine-to-inosine; TME: tumor microenvironment; BCa: bladder cancer; GSVA: Gene set variation analysis; RMS: RNA modification “writers” score; DEGs: differentially expressed genes; PCA: principal component analysis; HR: hazard ratio; 95% CI: 95% confidence interval; TMB: tumor mutation burden; m^7G: N^7-methylguanosine; Am: 2’-O-methyladenosine; snRNAs: small nuclear RNAs; 3’UTR: 3’-untranslated region; miRNA: microRNA; ceRNA: competing endogenous RNA; PAS: proximal polyA sites; ADAR: adenosine deaminase acting on RNA; ICB: Immune-checkpoint blockade; PD-1: programmed cell death-1; DC: dendritic cell; UCSC: University of California Santa Cruz; CNA: somatic copy number variation; miRNA-seq: miRNA-sequencing; RNA-seq: RNA-sequencing; TCGA-BLCA: The Cancer Genome Atlas-Bladder Urothelial Carcinoma; OS: overall survival; GEO: Gene-Expression Omnibus; WGCNA: Weighted gene co-expression network analysis; TMA: tissue microarray; IHC: Immunohistochemistry; UC: urothelial carcinoma; TMM: Trimmed Mean of M; GO: Gene Ontology; MSigDB: Molecular Signature Database; FC: fold change; FDR: false discovery rate; LASSO: least absolute shrinkage and selection operator; SD: standard deviation; EMT: epithelial-mesenchymal transition; Pan-FTBRS: pan-fibroblast TGF-β response signature; DDR: DNA damage repair; C-index: concordance index; ROC: receiver operating characteristic; AUC: an area under the curve; DEMs: differentially expressed miRNAs; KEGG: Kyoto Encyclopedia of Genes and Genomes; PDUI: Percentage of Distal polyA site Usage Index; TISIDB: Tumor and Immune System Interaction Database; GSEA: gene set enrichment analysis; “Writers” ^{MUT}: “writers” mutated; “Writers” ^{WT}: “writers”

wild-type; NK cells: natural killer cells; MDSC: Myeloid derived suppressor cell; SCC: squamous cell carcinoma; NES: normalized enrichment score; CR: complete response; PR: partial response; SD: stable disease; PD: progressive disease; Th17 cell: Type 17 T helper cell; DSS: disease-specific survival; RFS: recurrence-free survival; CSCC: cervical squamous cell carcinoma; ADC: antibody-drug conjugates.

Declarations

Availability of data and material

Data and download URLs involved in this study had been described in detail in the materials and methods section.

Author contributions

YH Huang, JP Yun, ZY Zhang and P Chen designed/planned the study and drafted the manuscript. ZY Zhang and P Chen acquired and analyzed data, performed computational modeling. ZY Zhang, P Chen, FY Liu, CS Lin, R Deng, LY Wu and Y Cao performed imaging analysis. All authors participated in discussion of related data and approved the submitted version.

Funding

This work was supported by the National Natural Science Foundation of China (No. 82072611 and No. 81872012 to JP Yun).

Acknowledgments

The authors of this study have no contribution to TCGA and GEO data collection. We would like to thank the TCGA and GEO database for open access.

Ethical approval

The studies involving human participants were reviewed and approved by the medical ethics committee of Sun Yat-sen University Cancer Center. The patients/participants provided their written informed consent to participate in this study.

Consent to participate

All authors voluntarily participated in this study.

Consent for publication

All authors agreed to the publication of this paper.

Competing interests

The authors declare no competing interests.

References

1. Richters A, Aben KKH, Kiemeney L. The global burden of urinary bladder cancer: an update[J]. World J Urol. 2020;38(8):1895–904.
2. Siegel RL, Miller KD, Jemal A. Cancer statistics, 2019[J]. CA Cancer J Clin. 2019;69(1):7–34.
3. Lenis AT, Lec PM, Chamie K, et al. Bladder Cancer: A Review[J] Jama. 2020;324(19):1980–91.
4. Babjuk M. Bladder Cancer in the Elderly[J]. Eur Urol. 2018;73(1):51–2.
5. Dobruch J, Daneshmand S, Fisch M, et al. Gender and Bladder Cancer: A Collaborative Review of Etiology, Biology, and Outcomes[J]. Eur Urol. 2016;69(2):300–10.
6. Freedman ND, Silverman DT, Hollenbeck AR, et al. Association between smoking and risk of bladder cancer among men and women[J]. JAMA. 2011;306(7):737–45.
7. Dominguez-Gutierrez PR, Kwenda EP, Donelan W, et al. Hyal2 Expression in Tumor-Associated Myeloid Cells Mediates Cancer-Related Inflammation in Bladder Cancer[J]. Cancer Res. 2021;81(3):648–57.
8. Moschini M, Zaffuto E, Karakiewicz PI, et al. External Beam Radiotherapy Increases the Risk of Bladder Cancer When Compared with Radical Prostatectomy in Patients Affected by Prostate Cancer: A Population-based Analysis[J]. Eur Urol. 2019;75(2):319–28.
9. Knight A, Askling J, Granath F, et al. Urinary bladder cancer in Wegener's granulomatosis: risks and relation to cyclophosphamide[J]. Ann Rheum Dis. 2004;63(10):1307–11.
10. Carlo MI, Ravichandran V, Srinavasan P, et al. Cancer Susceptibility Mutations in Patients With Urothelial Malignancies[J]. J Clin Oncol. 2020;38(5):406–14.
11. Zhang Z, Tang H, Chen P, et al. Demystifying the manipulation of host immunity, metabolism, and extraintestinal tumors by the gut microbiome[J]. Signal Transduct Target Ther. 2019;4:41.
12. Dawson MA, Kouzarides T. Cancer epigenetics: from mechanism to therapy[J]. Cell. 2012;150(1):12–27.
13. Sullenger BA, Nair S. From the RNA world to the clinic[J]. Science. 2016;352(6292):1417–20.
14. Barbieri I, Kouzarides T. Role of RNA modifications in cancer[J]. Nat Rev Cancer. 2020;20(6):303–22.
15. Motorin Y, Helm M. RNA nucleotide methylation[J]. Wiley Interdiscip Rev RNA. 2011;2(5):611–31.
16. Dong Z, Cui H. The Emerging Roles of RNA Modifications in Glioblastoma[J]. Cancers (Basel), 2020, 12(3).
17. Xiang JF, Yang Q, Liu CX, et al. N(6)-Methyladenosines Modulate A-to-I RNA Editing[J]. Mol Cell. 2018;69(1):126–35.e6.
18. Liu N, Dai Q, Zheng G, et al. N(6)-methyladenosine-dependent RNA structural switches regulate RNA-protein interactions[J]. Nature. 2015;518(7540):560–4.

19. Tassinari V, Cesarini V, Tomaselli S, et al. ADAR1 is a new target of METTL3 and plays a pro-oncogenic role in glioblastoma by an editing-independent mechanism[J]. Genome Biol. 2021;22(1):51.
20. Roundtree IA, Evans ME, Pan T, et al. Dynamic RNA Modifications in Gene Expression Regulation[J]. Cell. 2017;169(7):1187–200.
21. Gilbert WV, Bell TA, Schaening C. Messenger RNA modifications: Form, distribution, and function[J]. Science. 2016;352(6292):1408–12.
22. Wei CM, Gershowitz A, Moss B. Methylated nucleotides block 5' terminus of HeLa cell messenger RNA[J]. Cell. 1975;4(4):379–86.
23. Zaccara S, Ries RJ, Jaffrey SR. Reading, writing and erasing mRNA methylation[J]. Nat Rev Mol Cell Biol. 2019;20(10):608–24.
24. Pendleton KE, Chen B, Liu K, et al. The U6 snRNA m(6)A Methyltransferase METTL16 Regulates SAM Synthetase Intron Retention[J]. Cell. 2017;169(5):824–35.e14.
25. Yu J, Chen M, Huang H, et al. Dynamic m6A modification regulates local translation of mRNA in axons[J]. Nucleic Acids Res. 2018;46(3):1412–23.
26. Wei C, Gershowitz A, Moss B. N6, O2'-dimethyladenosine a novel methylated ribonucleoside next to the 5' terminal of animal cell and virus mRNAs[J]. Nature. 1975;257(5523):251–3.
27. Chen H, Gu L, Orellana EA, et al. METTL4 is an snRNA m(6)Am methyltransferase that regulates RNA splicing[J]. Cell Res. 2020;30(6):544–7.
28. Sendinc E, Valle-Garcia D, Dhall A, et al. PCIF1 Catalyzes m6Am mRNA Methylation to Regulate Gene Expression[J]. Mol Cell. 2019;75(3):620–30.e9.
29. Gu L, Wang L, Chen H, et al. CG14906 (mettl4) mediates m(6)A methylation of U2 snRNA in Drosophila[J]. Cell Discov. 2020;6:44.
30. Goh YT, Koh CWQ, Sim DY, et al. METTL4 catalyzes m6Am methylation in U2 snRNA to regulate pre-mRNA splicing[J]. Nucleic Acids Res. 2020;48(16):9250–61.
31. Safra M, Sas-Chen A, Nir R, et al. The m1A landscape on cytosolic and mitochondrial mRNA at single-base resolution[J]. Nature. 2017;551(7679):251–5.
32. Scheitl CPM, Ghaem Maghami M, Lenz AK, et al. Site-specific RNA methylation by a methyltransferase ribozyme[J]. Nature. 2020;587(7835):663–7.
33. Dominissini D, Nachtergaele S, Moshitch-Moshkovitz S, et al. The dynamic N(1)-methyladenosine methylome in eukaryotic messenger RNA[J]. Nature. 2016;530(7591):441–6.
34. Zhang C, Jia G. Reversible RNA, Modification. N(1)-methyladenosine (m(1)A) in mRNA and tRNA[J]. Genomics Proteom Bioinf. 2018;16(3):155–61.
35. Hauenschild R, Tserovski L, Schmid K, et al. The reverse transcription signature of N-1-methyladenosine in RNA-Seq is sequence dependent[J]. Nucleic Acids Res. 2015;43(20):9950–64.
36. Tian B, Hu J, Zhang H, et al. A large-scale analysis of mRNA polyadenylation of human and mouse genes[J]. Nucleic Acids Res. 2005;33(1):201–12.

37. Zhang Y, Liu L, Qiu Q, et al. Alternative polyadenylation: methods, mechanism, function, and role in cancer[J]. J Exp Clin Cancer Res. 2021;40(1):51.
38. Tian B, Manley JL. Alternative polyadenylation of mRNA precursors[J]. Nat Rev Mol Cell Biol. 2017;18(1):18–30.
39. Schönemann L, Kühn U, Martin G, et al. Reconstitution of CPSF active in polyadenylation: recognition of the polyadenylation signal by WDR33[J]. Genes Dev. 2014;28(21):2381–93.
40. Jang S, Cook NJ, Pye VE, et al. Differential role for phosphorylation in alternative polyadenylation function versus nuclear import of SR-like protein CPSF6[J]. Nucleic Acids Res. 2019;47(9):4663–83.
41. Brumbaugh J, Di Stefano B, Wang X, et al. Nudt21 Controls Cell Fate by Connecting Alternative Polyadenylation to Chromatin Signaling[J]. Cell. 2018;172(1–2):106–20.e21.
42. Xiang Y, Ye Y, Lou Y, et al. Comprehensive Characterization of Alternative Polyadenylation in Human Cancer[J]. J Natl Cancer Inst. 2018;110(4):379–89.
43. Xia Z, Donehower LA, Cooper TA, et al. Dynamic analyses of alternative polyadenylation from RNA-seq reveal a 3'-UTR landscape across seven tumour types[J]. Nat Commun. 2014;5:5274.
44. Park HJ, Ji P, Kim S, et al. 3' UTR shortening represses tumor-suppressor genes in trans by disrupting ceRNA crosstalk[J]. Nat Genet. 2018;50(6):783–9.
45. Fischl H, Neve J, Wang Z, et al. hnRNPC regulates cancer-specific alternative cleavage and polyadenylation profiles[J]. Nucleic Acids Res. 2019;47(14):7580–91.
46. Chu Y, Elrod N, Wang C, et al. Nudt21 regulates the alternative polyadenylation of Pak1 and is predictive in the prognosis of glioblastoma patients[J]. Oncogene. 2019;38(21):4154–68.
47. Peng X, Xu X, Wang Y, et al. A-to-I RNA Editing Contributes to Proteomic Diversity in Cancer[J]. Cancer Cell. 2018;33(5):817–28.e7.
48. Eisenberg E, Levanon EY. A-to-I. RNA editing - immune protector and transcriptome diversifier[J]. Nat Rev Genet. 2018;19(8):473–90.
49. Choudhury Y, Tay FC, Lam DH, et al. Attenuated adenosine-to-inosine editing of microRNA-376a* promotes invasiveness of glioblastoma cells[J]. J Clin Invest. 2012;122(11):4059–76.
50. Xu X, Wang Y, Mojumdar K, et al. A-to-I-edited miRNA-379-5p inhibits cancer cell proliferation through CD97-induced apoptosis[J]. J Clin Invest. 2019;129(12):5343–56.
51. Han SW, Kim HP, Shin JY, et al. RNA editing in RHOQ promotes invasion potential in colorectal cancer[J]. J Exp Med. 2014;211(4):613–21.
52. Bellmunt J, De Wit R, Vaughn DJ, et al. Pembrolizumab as Second-Line Therapy for Advanced Urothelial Carcinoma[J]. N Engl J Med. 2017;376(11):1015–26.
53. Balar AV, Castellano D, O'donnell PH, et al. First-line pembrolizumab in cisplatin-ineligible patients with locally advanced and unresectable or metastatic urothelial cancer (KEYNOTE-052): a multicentre, single-arm, phase 2 study[J]. Lancet Oncol. 2017;18(11):1483–92.
54. Tong J, Wang X, Liu Y, et al. Pooled CRISPR screening identifies m(6)A as a positive regulator of macrophage activation[J]. Sci Adv, 2021, 7(18).

55. Li HB, Tong J, Zhu S, et al. m(6)A mRNA methylation controls T cell homeostasis by targeting the IL-7/STAT5/SOCS pathways[J]. Nature. 2017;548(7667):338–42.
56. Wang H, Hu X, Huang M, et al. Mettl3-mediated mRNA m(6)A methylation promotes dendritic cell activation[J]. Nat Commun. 2019;10(1):1898.
57. Dong S, Wu Y, Liu Y, et al. N(6) -methyladenosine Steers RNA Metabolism and Regulation in Cancer[J]. Cancer Commun (Lond), 2021.
58. Golubnitschaja O, Kinkorova J, Costigliola V, Predictive. Preventive and Personalised Medicine as the hardcore of 'Horizon 2020': EPMA position paper[J]. Epma j. 2014;5(1):6.
59. Golubnitschaja O, Baban B, Boniolo G, et al. Medicine in the early twenty-first century: paradigm and anticipation - EPMA position paper 2016[J]. Epma j. 2016;7(1):23.
60. Brunmair J, Bileck A, Stimpfl T, et al. Metabo-tip: a metabolomics platform for lifestyle monitoring supporting the development of novel strategies in predictive, preventive and personalised medicine[J]. Epma j. 2021;12(2):141–53.
61. Kucera R, Pecen L, Topolcan O, et al. Prostate cancer management: long-term beliefs, epidemic developments in the early twenty-first century and 3PM dimensional solutions[J]. Epma j. 2020;11(3):399–418.
62. Yuan Y, Yang C, Wang Y, et al. Functional metabolome profiling may improve individual outcomes in colorectal cancer management implementing concepts of predictive, preventive, and personalized medical approach[J]. Epma j. 2022;13(1):39–55.
63. Park JG, Choi BK, Lee Y, et al. Plasma complement C7 as a target in non-small cell lung cancer patients to implement 3P medicine strategies[J]. Epma j. 2021;12(4):629–45.
64. Ran Y, He J, Peng W, et al. Development and validation of a transcriptomic signature-based model as the predictive, preventive, and personalized medical strategy for preterm birth within 7 days in threatened preterm labor women[J]. Epma j. 2022;13(1):87–106.
65. Bizzarri M, Fedeli V, Monti N, et al. Personalization of medical treatments in oncology: time for rethinking the disease concept to improve individual outcomes[J]. Epma j. 2021;12(4):545–58.
66. Mayakonda A, Lin DC, Assenov Y, et al. Maftools: efficient and comprehensive analysis of somatic variants in cancer[J]. Genome Res. 2018;28(11):1747–56.
67. Davis S, Meltzer PS. GEOquery: a bridge between the Gene Expression Omnibus (GEO) and BioConductor[J]. Bioinformatics. 2007;23(14):1846–7.
68. Kim WJ, Kim EJ, Kim SK, et al. Predictive value of progression-related gene classifier in primary non-muscle invasive bladder cancer[J]. Mol Cancer. 2010;9:3.
69. Lee JS, Leem SH, Lee SY, et al. Expression signature of E2F1 and its associated genes predict superficial to invasive progression of bladder tumors[J]. J Clin Oncol. 2010;28(16):2660–7.
70. Sjödahl G, Lauss M, Lövgren K, et al. A molecular taxonomy for urothelial carcinoma[J]. Clin Cancer Res. 2012;18(12):3377–86.

71. Lindgren D, Sjödahl G, Lauss M, et al. Integrated genomic and gene expression profiling identifies two major genomic circuits in urothelial carcinoma[J]. PLoS ONE. 2012;7(6):e38863.
72. Sjödahl G, Eriksson P, Patschan O, et al. Molecular changes during progression from nonmuscle invasive to advanced urothelial carcinoma[J]. Int J Cancer. 2020;146(9):2636–47.
73. Riester M, Taylor JM, Feifer A, et al. Combination of a novel gene expression signature with a clinical nomogram improves the prediction of survival in high-risk bladder cancer[J]. Clin Cancer Res. 2012;18(5):1323–33.
74. Riester M, Werner L, Bellmunt J, et al. Integrative analysis of 1q23.3 copy-number gain in metastatic urothelial carcinoma[J]. Clin Cancer Res. 2014;20(7):1873–83.
75. Choi W, Porten S, Kim S, et al. Identification of distinct basal and luminal subtypes of muscle-invasive bladder cancer with different sensitivities to frontline chemotherapy[J]. Cancer Cell. 2014;25(2):152–65.
76. Guo CC, Bondaruk J, Yao H, et al. Assessment of Luminal and Basal Phenotypes in Bladder Cancer[J]. Sci Rep. 2020;10(1):9743.
77. Therkildsen C, Eriksson P, Höglund M, et al. Molecular subtype classification of urothelial carcinoma in Lynch syndrome[J]. Mol Oncol. 2018;12(8):1286–95.
78. Sjödahl G, Eriksson P, Liedberg F, et al. Molecular classification of urothelial carcinoma: global mRNA classification versus tumour-cell phenotype classification[J]. J Pathol. 2017;242(1):113–25.
79. Leek JT, Johnson WE, Parker HS, et al. The sva package for removing batch effects and other unwanted variation in high-throughput experiments[J]. Bioinformatics. 2012;28(6):882–3.
80. Langfelder P, Horvath S. WGCNA: an R package for weighted correlation network analysis[J]. BMC Bioinformatics. 2008;9:559.
81. Zhang Z, Chen P, Xie H, et al. Overexpression of GINS4 Is Associated With Tumor Progression and Poor Survival in Hepatocellular Carcinoma[J]. Front Oncol. 2021;11:654185.
82. Mariathasan S, Turley SJ, Nickles D, et al. TGFβ attenuates tumour response to PD-L1 blockade by contributing to exclusion of T cells[J]. Nature. 2018;554(7693):544–8.
83. Snyder A, Nathanson T, Funt SA, et al. Contribution of systemic and somatic factors to clinical response and resistance to PD-L1 blockade in urothelial cancer: An exploratory multi-omic analysis[J]. PLoS Med. 2017;14(5):e1002309.
84. Ulloa-Montoya F, Louahed J, Dizier B, et al. Predictive gene signature in MAGE-A3 antigen-specific cancer immunotherapy[J]. J Clin Oncol. 2013;31(19):2388–95.
85. Wilkerson MD, Hayes DN. ConsensusClusterPlus: a class discovery tool with confidence assessments and item tracking[J]. Bioinformatics. 2010;26(12):1572–3.
86. Hänzelmann S, Castelo R, Guinney J. GSVA: gene set variation analysis for microarray and RNA-seq data[J]. BMC Bioinformatics. 2013;14:7.
87. Subramanian A, Tamayo P, Mootha VK, et al. Gene set enrichment analysis: a knowledge-based approach for interpreting genome-wide expression profiles[J]. Proc Natl Acad Sci U S A.

2005;102(43):15545–50.
88. Yu G, Wang LG, Han Y, et al. clusterProfiler: an R package for comparing biological themes among gene clusters[J]. Omics. 2012;16(5):284–7.
89. Ritchie ME, Phipson B, Wu D, et al. limma powers differential expression analyses for RNA-sequencing and microarray studies[J]. Nucleic Acids Res. 2015;43(7):e47.
90. Engebretsen S, Bohlin J. Statistical predictions with glmnet[J]. Clin Epigenetics. 2019;11(1):123.
91. Gui J, Li H. Penalized Cox regression analysis in the high-dimensional and low-sample size settings, with applications to microarray gene expression data[J]. Bioinformatics. 2005;21(13):3001–8.
92. Long J, Wang A, Bai Y, et al. Development and validation of a TP53-associated immune prognostic model for hepatocellular carcinoma[J]. EBioMedicine. 2019;42:363–74.
93. Chen P, Zhang Z, Chen X. Overexpression of PKMYT1 Facilitates Tumor Development and Is Correlated with Poor Prognosis in Clear Cell Renal Cell Carcinoma[J]. Med Sci Monit. 2020;26:e926755.
94. Liu CJ, Hu FF, Xia MX, et al. GSCALite: a web server for gene set cancer analysis[J]. Bioinformatics. 2018;34(21):3771–2.
95. Yang W, Soares J, Greninger P, et al. Genomics of Drug Sensitivity in Cancer (GDSC): a resource for therapeutic biomarker discovery in cancer cells[J]. Nucleic Acids Res. 2013;41(Database issue):D955-61.
96. Ru B, Wong CN, Tong Y, et al. TISIDB: an integrated repository portal for tumor-immune system interactions[J]. Bioinformatics. 2019;35(20):4200–2.
97. Glickman ME, Rao SR, Schultz MR. False discovery rate control is a recommended alternative to Bonferroni-type adjustments in health studies[J]. J Clin Epidemiol. 2014;67(8):850–7.
98. Marceca GP, Tomasello L, Distefano R, et al. Detecting and Characterizing A-To-I microRNA Editing in Cancer[J]. Cancers (Basel), 2021, 13(7).
99. Elkon R, Ugalde AP, Agami R. Alternative cleavage and polyadenylation: extent, regulation and function[J]. Nat Rev Genet. 2013;14(7):496–506.
100. Sebestyén E, Singh B, Miñana B, et al. Large-scale analysis of genome and transcriptome alterations in multiple tumors unveils novel cancer-relevant splicing networks[J]. Genome Res. 2016;26(6):732–44.
101. Lambert SA, Jolma A, Campitelli LF, et al. Hum Transcription Factors[J] Cell. 2018;172(4):650–65.
102. Da Rocha ST, Gendrel AV. The influence of DNA methylation on monoallelic expression[J]. Essays Biochem. 2019;63(6):663–76.
103. Wang J, Chen S. RACK1 promotes miR-302b/c/d-3p expression and inhibits CCNO expression to induce cell apoptosis in cervical squamous cell carcinoma[J]. Cancer Cell Int. 2020;20:385.
104. Bunjobpol W, Dulloo I, Igarashi K, et al. Suppression of acetylpolyamine oxidase by selected AP-1 members regulates DNp73 abundance: mechanistic insights for overcoming DNp73-mediated resistance to chemotherapeutic drugs[J]. Cell Death Differ. 2014;21(8):1240–9.

105. Hafeez U, Parakh S, Gan HK, et al. Antibody-Drug Conjugates for Cancer Therapy[J]. Molecules, 2020, 25(20).
106. Starodub AN, Ocean AJ, Shah MA, et al. First-in-Human Trial of a Novel Anti-Trop-2 Antibody-SN-38 Conjugate, Sacituzumab Govitecan, for the Treatment of Diverse Metastatic Solid Tumors[J]. Clin Cancer Res. 2015;21(17):3870–8.
107. Modi S, Saura C, Yamashita T, et al. Trastuzumab Deruxtecan in Previously Treated HER2-Positive Breast Cancer[J]. N Engl J Med. 2020;382(7):610–21.
108. Krop IE, Beeram M, Modi S, et al. Phase I study of trastuzumab-DM1, an HER2 antibody-drug conjugate, given every 3 weeks to patients with HER2-positive metastatic breast cancer[J]. J Clin Oncol. 2010;28(16):2698–704.
109. Trudel S, Lendvai N, Popat R, et al. Antibody-drug conjugate, GSK2857916, in relapsed/refractory multiple myeloma: an update on safety and efficacy from dose expansion phase I study[J]. Blood Cancer J. 2019;9(4):37.
110. Wynne J, Wright D, Stock W. Inotuzumab: from preclinical development to success in B-cell acute lymphoblastic leukemia[J]. Blood Adv. 2019;3(1):96–104.
111. Senter PD, Sievers EL. The discovery and development of brentuximab vedotin for use in relapsed Hodgkin lymphoma and systemic anaplastic large cell lymphoma[J]. Nat Biotechnol. 2012;30(7):631–7.
112. Sehn LH, Herrera AF, Flowers CR, et al. Polatuzumab Vedotin in Relapsed or Refractory Diffuse Large B-Cell Lymphoma[J]. J Clin Oncol. 2020;38(2):155–65.
113. Bross PF, Beitz J, Chen G, et al. Approval summary: gemtuzumab ozogamicin in relapsed acute myeloid leukemia[J]. Clin Cancer Res. 2001;7(6):1490–6.
114. Zeng D, Li M, Zhou R, et al. Tumor Microenvironment Characterization in Gastric Cancer Identifies Prognostic and Immunotherapeutically Relevant Gene Signatures[J]. Cancer Immunol Res. 2019;7(5):737–50.
115. Rizvi NA, Hellmann MD, Snyder A, et al. Cancer immunology. Mutational landscape determines sensitivity to PD-1 blockade in non-small cell lung cancer[J]. Science. 2015;348(6230):124–8.
116. Le DT, Durham JN, Smith KN, et al. Mismatch repair deficiency predicts response of solid tumors to PD-1 blockade[J]. Science. 2017;357(6349):409–13.
117. Chen DS, Mellman I. Elements of cancer immunity and the cancer-immune set point[J]. Nature. 2017;541(7637):321–30.
118. Lan T, Li H, Zhang D, et al. KIAA1429 contributes to liver cancer progression through N6-methyladenosine-dependent post-transcriptional modification of GATA3[J]. Mol Cancer. 2019;18(1):186.
119. Shen P, Yang T, Chen Q, et al. CircNEIL3 regulatory loop promotes pancreatic ductal adenocarcinoma progression via miRNA sponging and A-to-I RNA-editing[J]. Mol Cancer. 2021;20(1):51.

120. Zhang T, Cooper S, Brockdorff N. The interplay of histone modifications - writers that read[J]. EMBO Rep. 2015;16(11):1467–81.
121. Zhou J, Wang J, Hong B, et al. Gene signatures and prognostic values of m6A regulators in clear cell renal cell carcinoma - a retrospective study using TCGA database[J]. Aging. 2019;11(6):1633–47.
122. Xing J, Shen S, Dong Z, et al. Analysis of Multi-Layer RNA Modification Patterns for the Characterization of Tumor Immune Microenvironment in Hepatocellular Carcinoma[J]. Front Cell Dev Biol. 2021;9:761391.
123. Chen H, Yao J, Bao R, et al. Cross-talk of four types of RNA modification writers defines tumor microenvironment and pharmacogenomic landscape in colorectal cancer[J]. Mol Cancer. 2021;20(1):29.
124. Qian JY, Gao J, Sun X, et al. KIAA1429 acts as an oncogenic factor in breast cancer by regulating CDK1 in an N6-methyladenosine-independent manner[J]. Oncogene. 2019;38(33):6123–41.
125. Tang J, Han T, Tong W, et al. N(6)-methyladenosine (m(6)A) methyltransferase KIAA1429 accelerates the gefitinib resistance of non-small-cell lung cancer[J]. Cell Death Discov. 2021;7(1):108.
126. Miao R, Dai CC, Mei L, et al. KIAA1429 regulates cell proliferation by targeting c-Jun messenger RNA directly in gastric cancer[J]. J Cell Physiol. 2020;235(10):7420–32.
127. Han Q, Yang J, Yang H, et al. KIAA1429 promotes osteosarcoma progression by promoting stem cell properties and is regulated by miR-143-3p[J]. Cell Cycle. 2020;19(10):1172–85.
128. Veglia F, Perego M, Gabrilovich D. Myeloid-derived suppressor cells coming of age[J]. Nat Immunol. 2018;19(2):108–19.
129. Schneider AK, Chevalier MF, Derré L. The multifaceted immune regulation of bladder cancer[J]. Nat Rev Urol. 2019;16(10):613–30.
130. Zhang H, Ye YL, Li MX, et al. CXCL2/MIF-CXCR2 signaling promotes the recruitment of myeloid-derived suppressor cells and is correlated with prognosis in bladder cancer[J]. Oncogene. 2017;36(15):2095–104.
131. Obermajer N, Muthuswamy R, Odunsi K, et al. PGE(2)-induced CXCL12 production and CXCR4 expression controls the accumulation of human MDSCs in ovarian cancer environment[J]. Cancer Res. 2011;71(24):7463–70.
132. Tavazoie MF, Pollack I, Tanqueco R, et al. LXR/ApoE Activation Restricts Innate Immune Suppression in Cancer[J]. Cell. 2018;172(4):825–40.e18.
133. Wang L, Yi T, Kortylewski M, et al. IL-17 can promote tumor growth through an IL-6-Stat3 signaling pathway[J]. J Exp Med. 2009;206(7):1457–64.
134. Wang L, Saci A, Szabo PM, et al. EMT- and stroma-related gene expression and resistance to PD-1 blockade in urothelial cancer[J]. Nat Commun. 2018;9(1):3503.
135. Majumder S, Crabtree JS, Golde TE, et al. Targeting Notch in oncology: the path forward[J]. Nat Rev Drug Discov. 2021;20(2):125–44.

136. Kwon OJ, Zhang L, Wang J, et al. Notch promotes tumor metastasis in a prostate-specific Pten-null mouse model[J]. J Clin Invest. 2016;126(7):2626–41.
137. Sethi N, Dai X, Winter CG, et al. Tumor-derived JAGGED1 promotes osteolytic bone metastasis of breast cancer by engaging notch signaling in bone cells[J]. Cancer Cell. 2011;19(2):192–205.
138. Dikiy S, Li J, Bai L, et al. A distal Foxp3 enhancer enables interleukin-2 dependent thymic Treg cell lineage commitment for robust immune tolerance[J]. Immunity. 2021;54(5):931–46.e11.
139. Johnson DE, O'keefe RA, Grandis JR. Targeting the IL-6/JAK/STAT3 signalling axis in cancer[J]. Nat Rev Clin Oncol. 2018;15(4):234–48.
140. Li N, Zhan X. Identification of pathology-specific regulators of m(6)A RNA modification to optimize lung cancer management in the context of predictive, preventive, and personalized medicine[J]. Epma j. 2020;11(3):485–504.
141. Kudela E, Liskova A, Samec M, et al. The interplay between the vaginal microbiome and innate immunity in the focus of predictive, preventive, and personalized medical approach to combat HPV-induced cervical cancer[J]. Epma j. 2021;12(2):199–220.

Figures

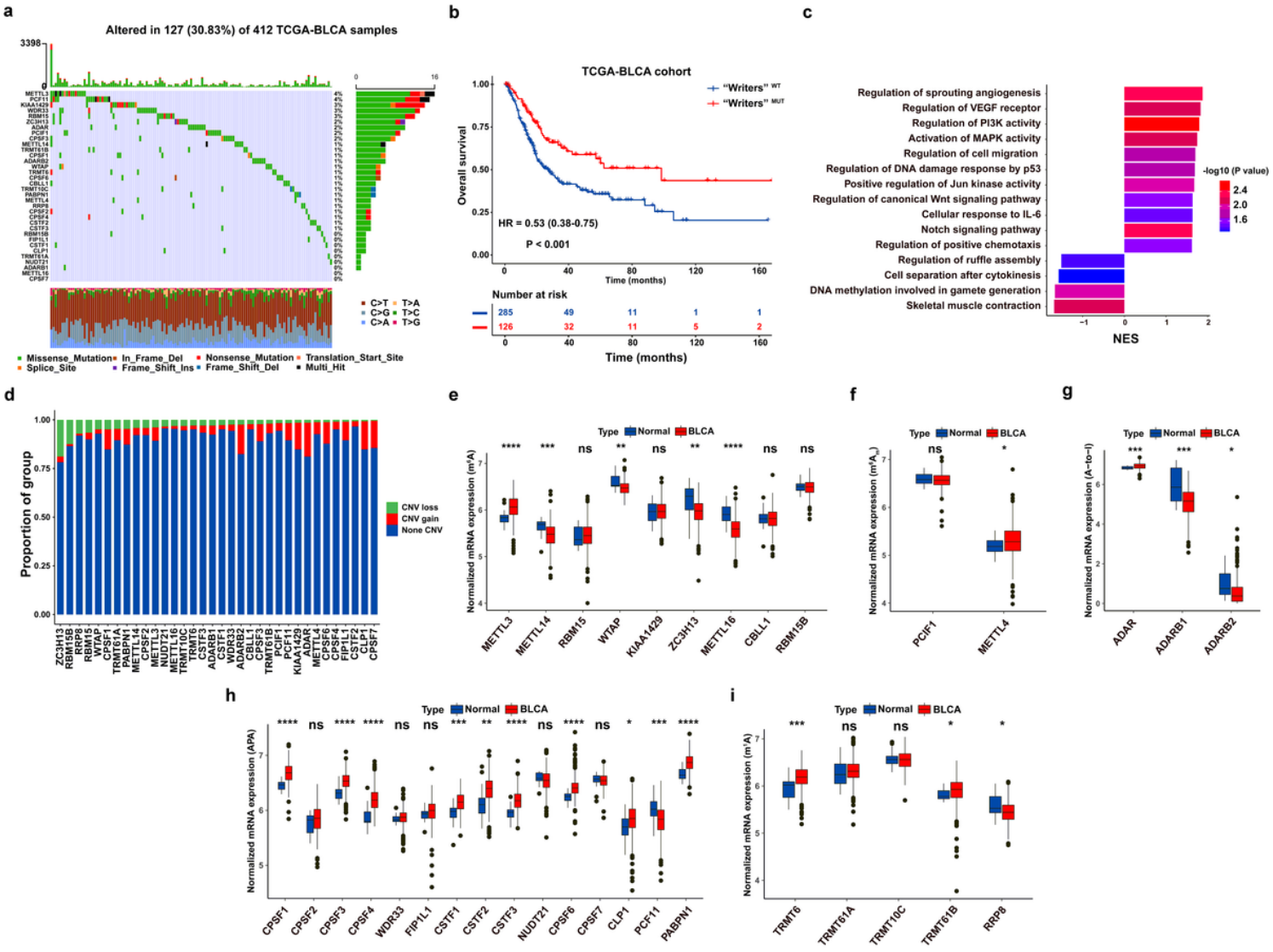

Figure 1

Genetic and transcriptional characteristics of RNA modification “writers” in the TCGA-BLCA cohort. (**a**) Waterfall plot showing mutation frequency of 34 “writers” in 412 BCa cases. The upper and the right bar chart represented the TMB for individual sample, and the proportion of mutation type of each “writer”, respectively. (**b**) Kaplan-Meier curve of OS in “Writers” ^{MUT} and “Writers” ^{WT} BCa patients. (**c**) Bar chart depicting significantly biological pathways enriched in “Writers” ^{WT} (Right) or “Writers” ^{MUT} (Left) BCa patients by GSEA. (**d**) Bar chart depicting CNV frequency of 34 RNA modification “writers”. (**e-i**) Boxplot representing mRNA levels of 34 “writers” between normal tissues and BCa samples, with P values derived from Wilcoxon rank sum test.

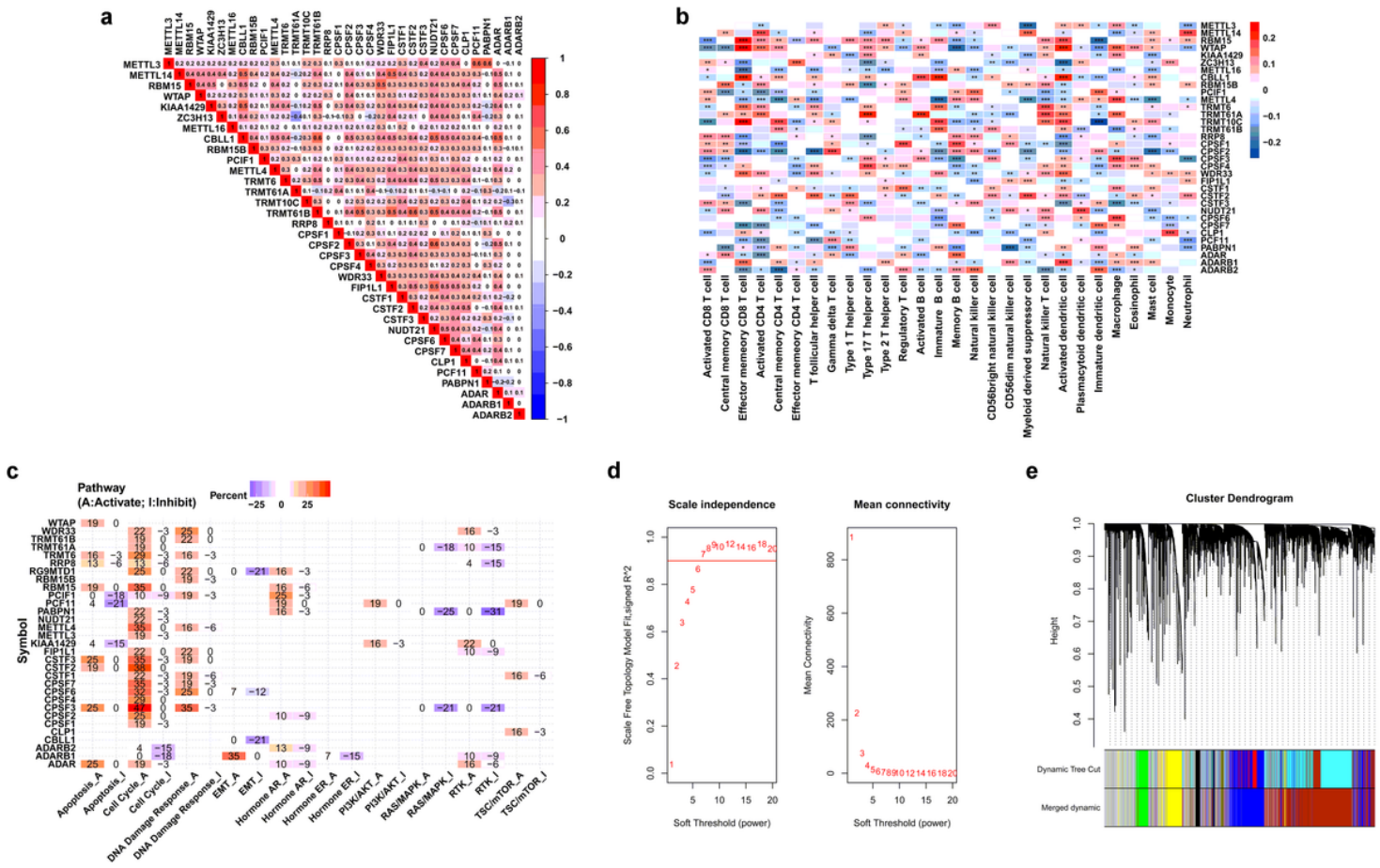

Figure 2

Prognosis and immune characteristics of RNA modification “writers” in BCa samples. (**a**) Heatmap showing the positive and negative correlations among 34 RNA modification “writers” in the TCGA-BLCA cohort. (**b**) Heatmap displaying the positive and negative correlations between 34 RNA modification “writers” and infiltrating proportions of 28 immune cells in the meta-GEO cohort. (**c**) Heatmap displaying “writers” with inhibitory (Blue) or activated (Red) functions in multiple pathways in BCa. (**d**) The scale-independence index and the mean connectivity for diverse soft threshold powers of the WGCNA. (**e**) Cluster dendrogram of prognosis-associated genes in the TCGA-BLCA using WGCNA method. Each branch in the figure and each color below represented one gene and one co-expression module, respectively.

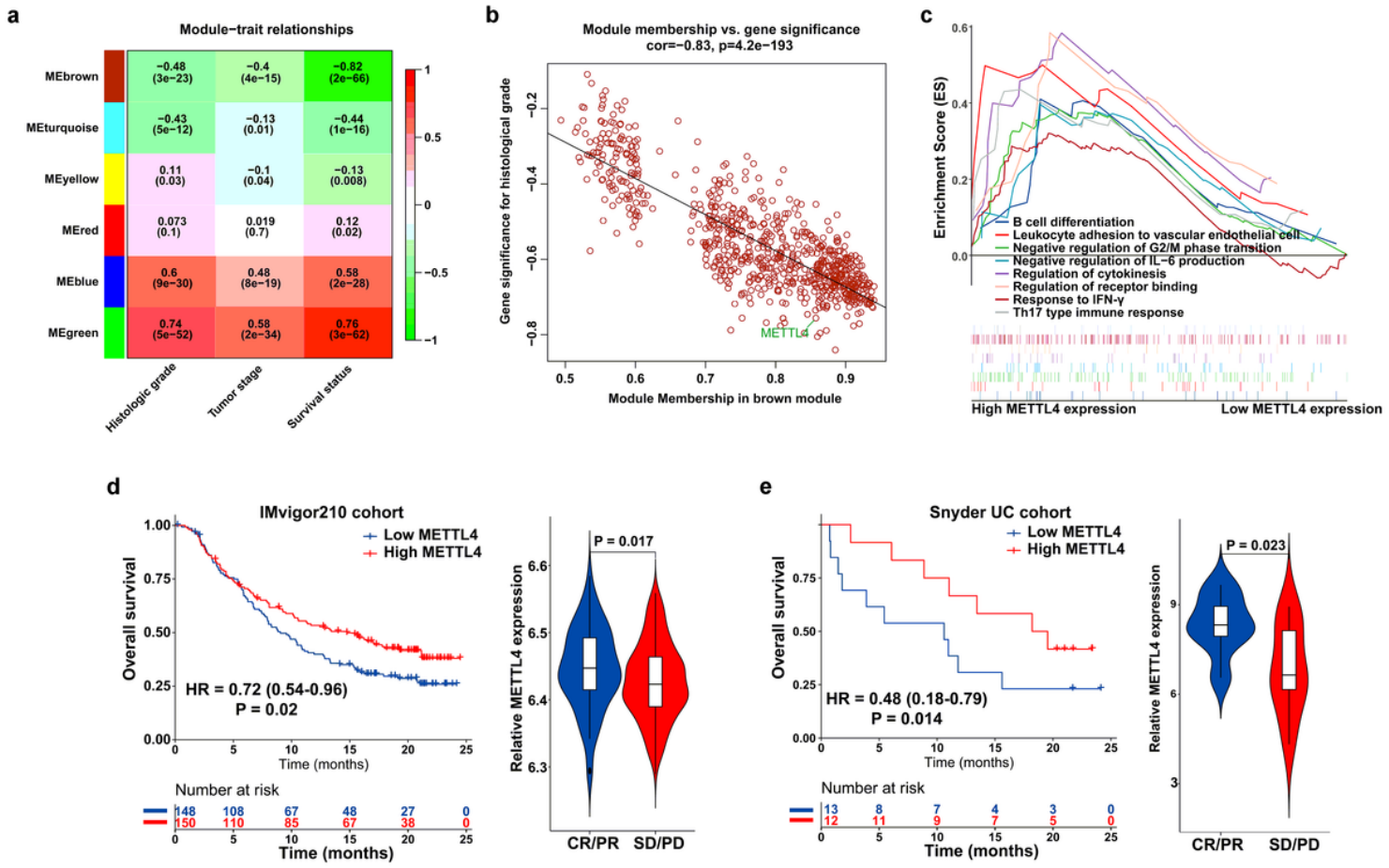

Figure 3

Prognosis and immune characteristics of METTL4 in BCa samples. (**a**) Heatmap illustrating the modules-trait correlation between module eigengenes and clinical traits using WGCNA method. (**b**) Scatter plots showing the correlation between GS and MM of genes in brown module using WGCNA method. (**c**) GSEA results of biological pathways clustered in high METTL4-expressing BCa patients in the meta-GEO cohort. Kaplan-Meier curve and violin plot illustrating the difference in OS and clinical response to immunotherapy of tumor patients between high and low METTL4-expressing group based on (**d**) IMvigor210 cohort and **(e)** Snyder UC cohort.

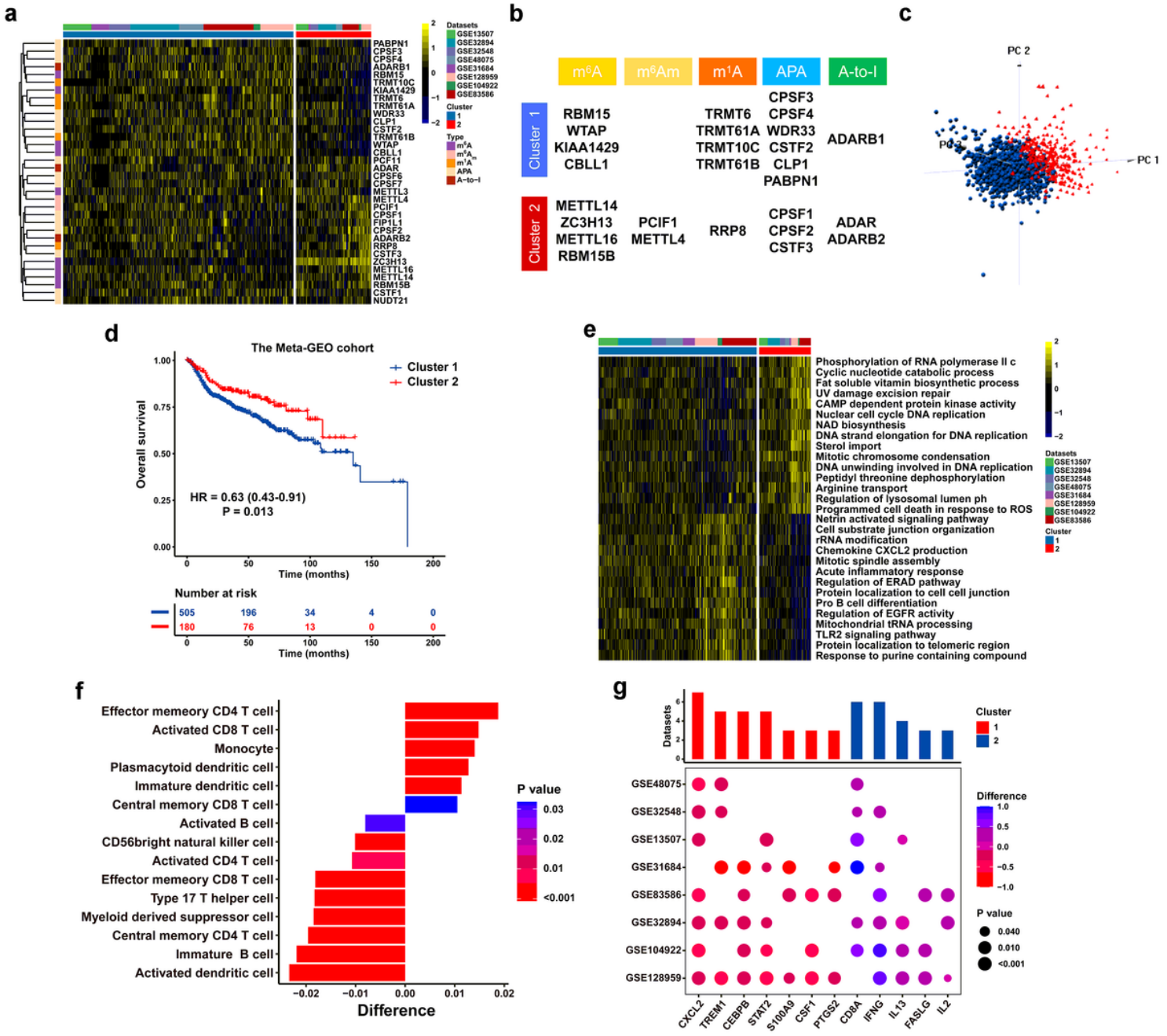

Figure 4

RNA modification patterns and their biological significance in the meta-GEO cohort. (**a**) Heatmap presenting unsupervised clustering results of 34 RNA modification "writers" in eight independent BCa cohorts. Each column and row represented patients and RNA modification "writers", respectively. (**b**) Specific distribution of 34 RNA modification "writers" enriched in two primary patterns. **(c)** PCA illustrating the expression of 34 RNA modification "writers" to distinguish two primary patterns in 1410 BCa patients. (**d**) Kaplan-Meier curve of patients' OS in two RNA modification patterns. (**e**) Heatmap displaying the difference in relatively activated biological processes between two distinct RNA modification patterns by GSVA. (**f**) Bar chart showing the proportion of immune cells between two clusters. Difference > 0 or < 0 represented the immune cells enriched in Cluster 2 or Cluster 1, respectively. (**g**) Difference in the expression of MDSCs and activated $CD8^+$ T cells marker genes between two clusters.

The upper bar chart represented the number of datasets that were significantly different between Cluster 1 and Cluster 2. The color and size bubble illustrated the difference in each GEO, and the statistical significance of difference, respectively. Difference > 0 or < 0 implied greater expression of immune cell marker genes in Cluster 2 or Cluster 1, respectively.

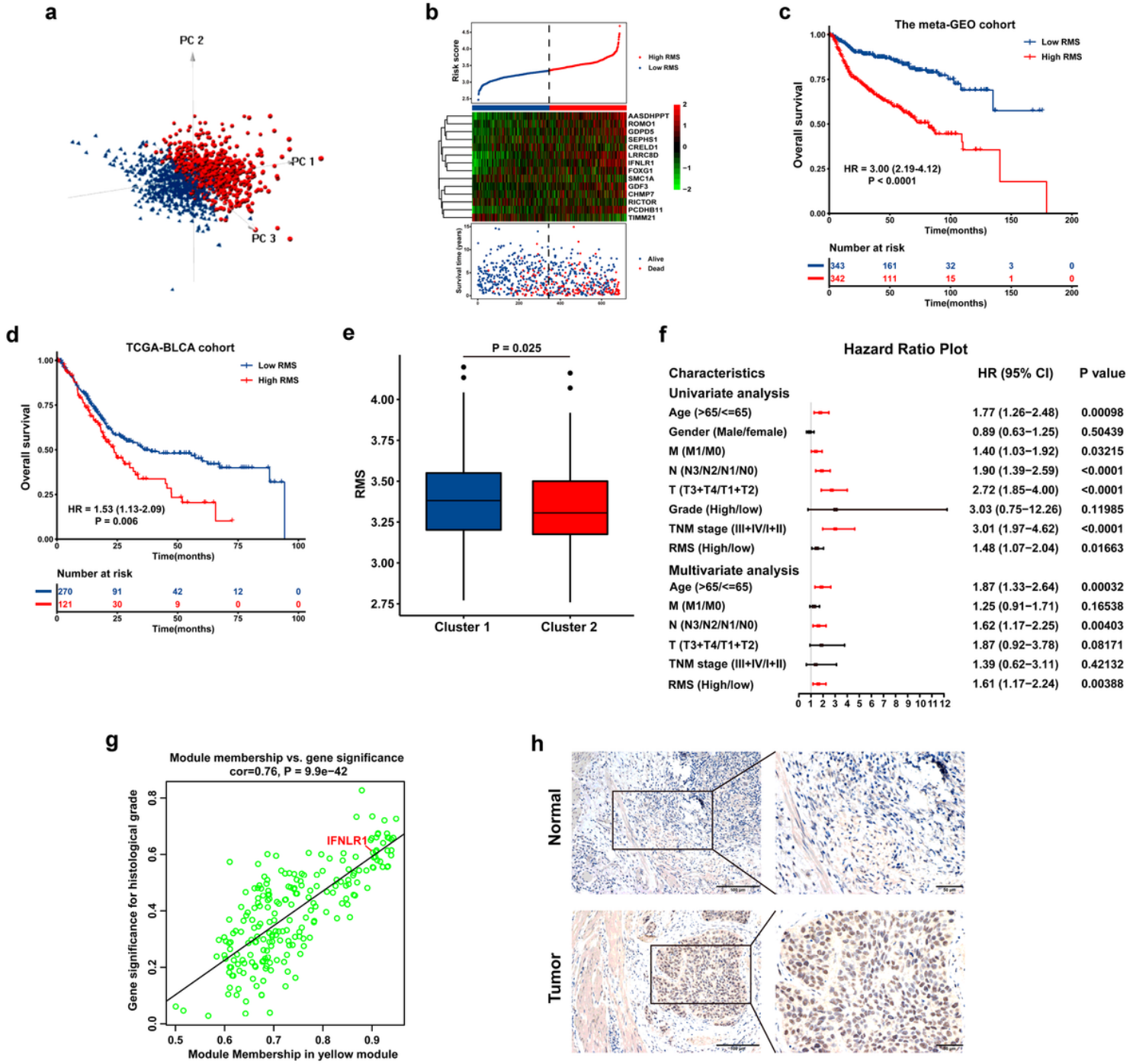

Figure 5

Construction and evaluation of the RMS model in BCa. (**a**) PCA exhibiting a remarkable distinction between cases with high or low risk score. (**b**) The risk score distribution, heatmap showing the expression of 14 DEGs, and survival status for each BCa case in the meta-GEO group. The black dotted

line indicated the RMS cutoff to classify cases into low- and high-risk groups. Kaplan-Meier curve revealing OS difference between RMS-high or -low patients in (**c**) the TCGA and (**d**) meta-GEO group. (**e**) Boxplots describing the RMS of two RNA modification patterns in the meta-GEO cohort. (**f**) Forest plot of Cox regression analysis to evaluate the relationship between the RMS and clinicopathological parameters. (**g**) Scatter plots showing the correlation between GS and MM of genes in green module using WGCNA method. (**h**) Representative IHC staining displaying the expression of IFNLR1 in tumor samples and adjacent tissues of BCa cases.

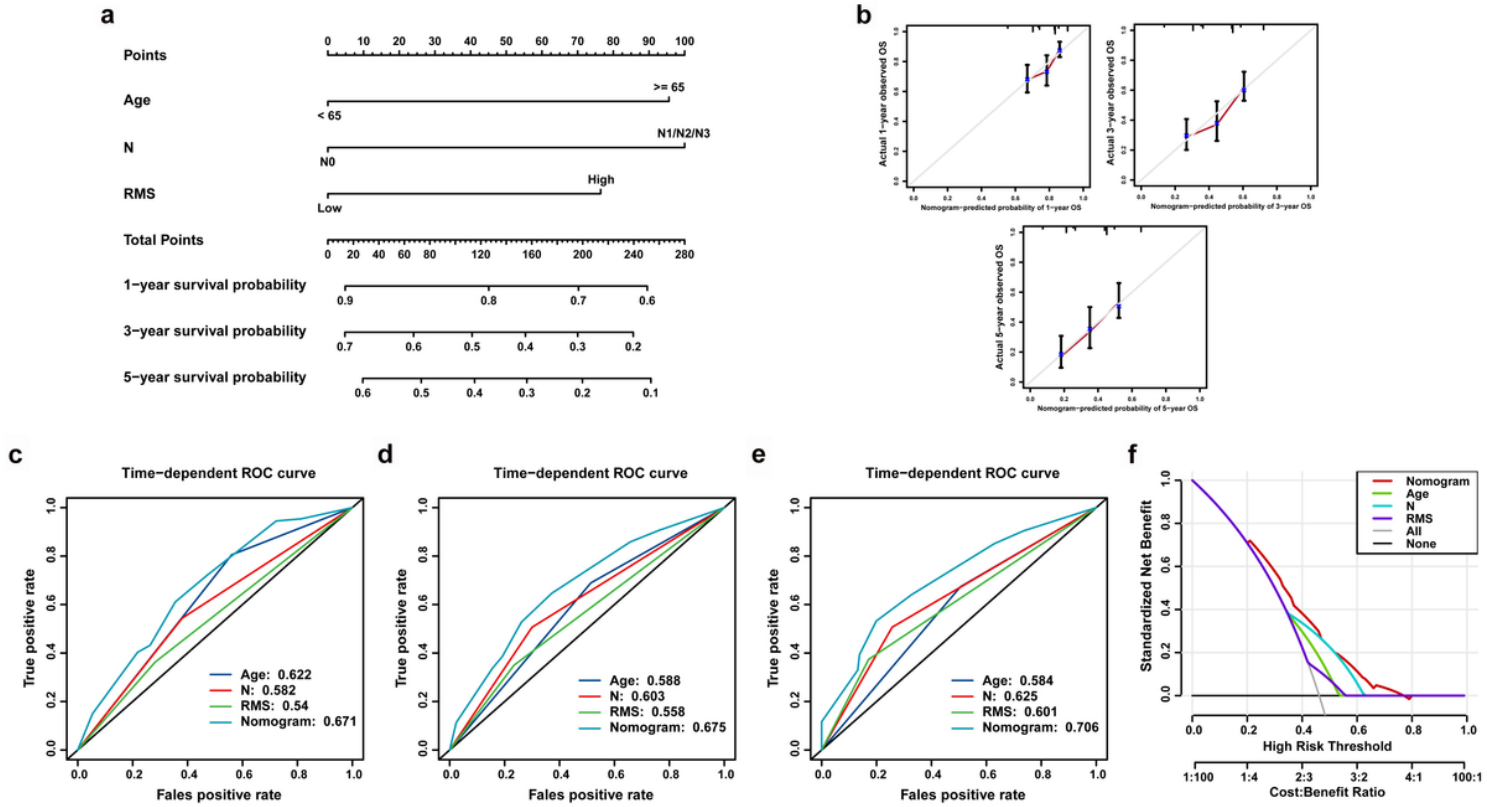

Figure 6

Construction and validation of nomogram model for survival prediction in BCa. (**a**) Nomogram for predicting the probability of 1-, 3-, and 5-year OS for BCa patients. (**b**) Calibration curve of nomogram to assess the consistency between predicted and observed 1-, 3-, and 5- year outcomes. Time-dependent ROC curve of the nomogram, N classification, age and the RMS for (**c**) 1-year, (**d**) 3-year, and (**e**) 5-year OS of BCa patients. (**f**) DCA curves of the nomogram model for BCa patients' survival.

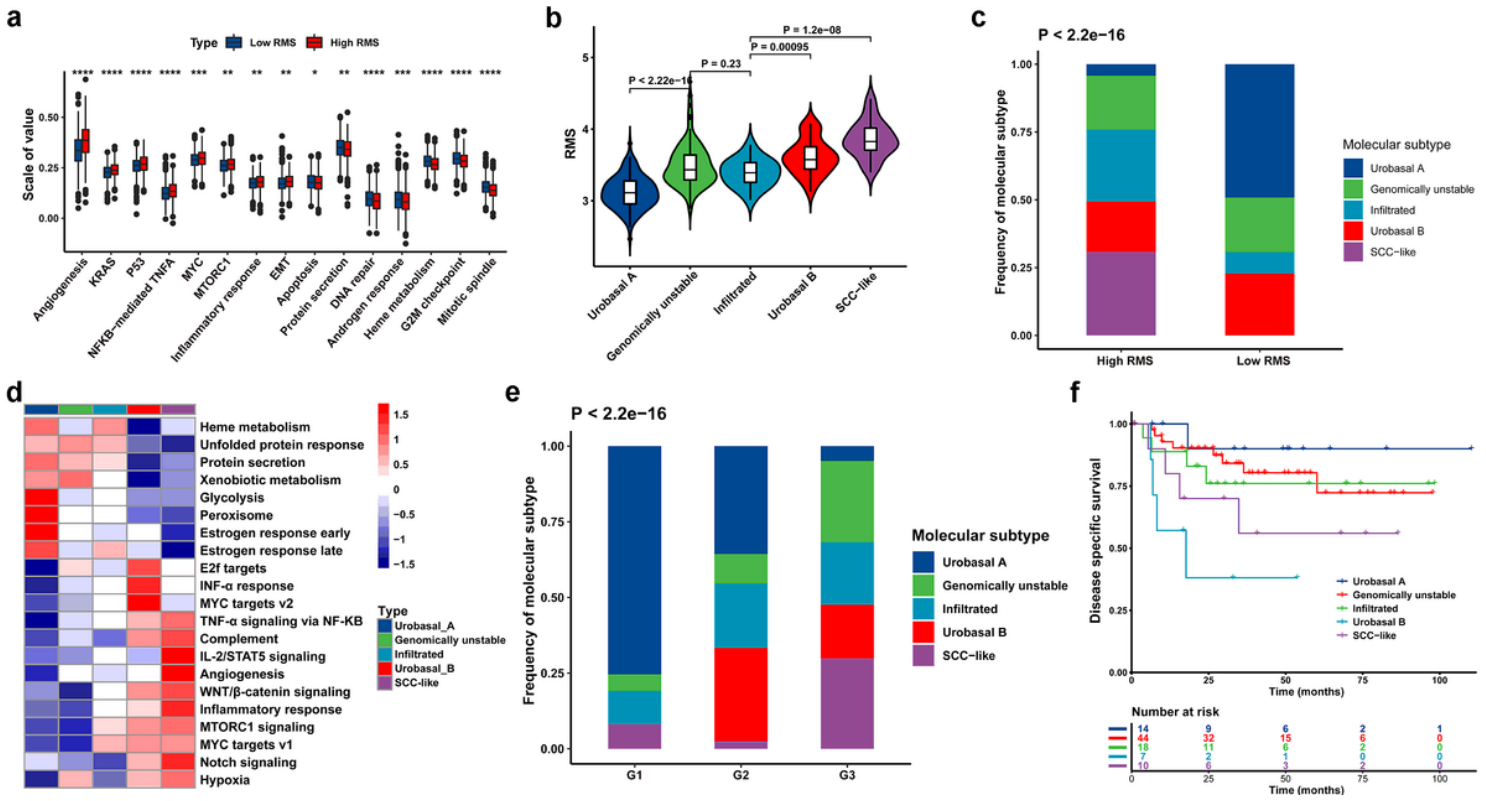

Figure 7

Biological function characteristics of the RMS model in BCa patients. (**a**) Boxplot representing the association between the RMS and known signatures based on the meta-GEO cohort. (**b**) Violin plot illustrating RMS distribution among five molecular subtypes based on GSE32894. (**c**) Bar chart describing difference in the distribution of five molecular subtypes between RMS-high and -low groups based on GSE32894 cohort. (**d**) Heatmap showing difference in the biological processes among five molecular subtypes. (**e**) Bar chart exhibiting difference in the distribution of histological grade among five molecular subtypes. (**f**) Kaplan-Meier curve revealing difference in OS among five molecular subtypes for BCa cases at histological grade 3.

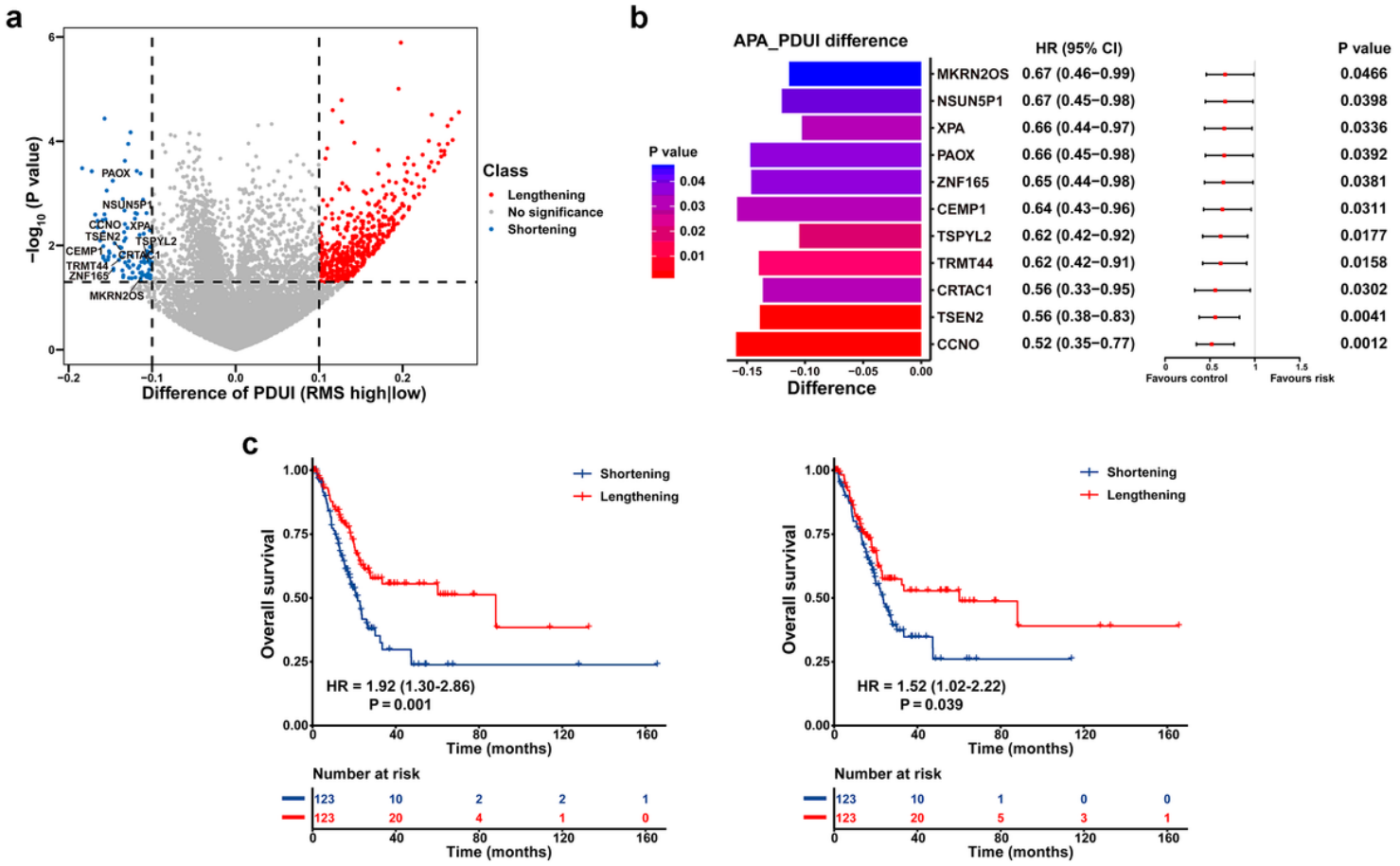

Figure 8

Post-transcriptional characteristics related to the RMS of BCa patients in the TCGA-BLCA cohort. (**a**) Volcano plot representing significantly differences in the PDUI of each gene between RMS-high and -low groups. (**b**) Bar graphs showing transcripts with shortening 3'UTR events in RMS-high group. Forest plots showing univariate Cox regression analysis for genes with differential PDUI between RMS-high and -low group. (**c**) Kaplan-Meier curve showing OS between PDUI lengthening and PDUI shortening of CCNO and PAOX.

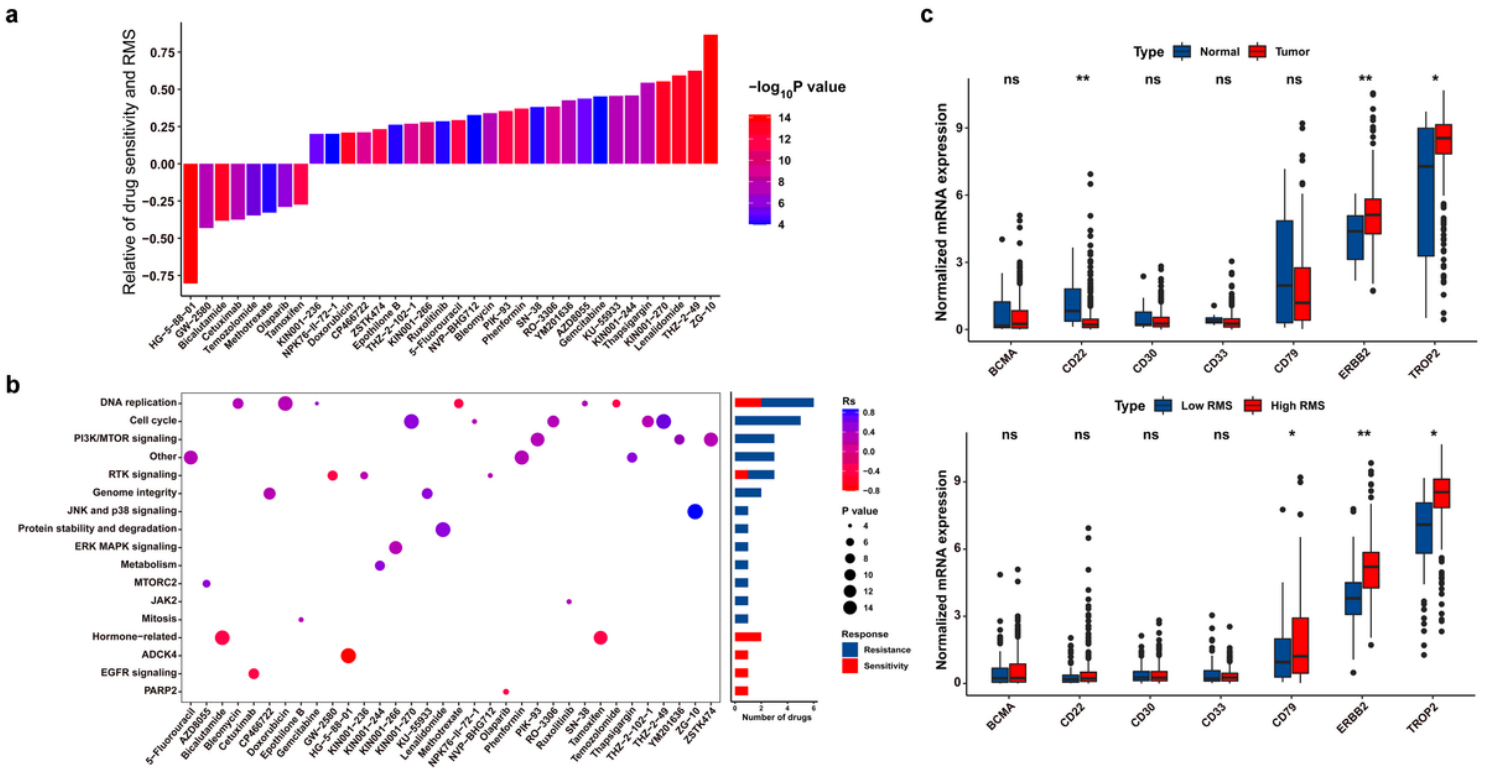

Figure 9

The association between the RMS and efficacy of antitumor chemotherapy. **(a)** Spearman correlation analysis between the RMS and drug sensitivity. The columns represented drugs. The brightness and height represented the significance and degree of the correlation, respectively. Rs > 0.2 or Rs < -0.2 indicated drug resistance or drug sensitivity, respectively. **(b)** Bar chart displaying signal pathways associated with drugs that were resistant (Blue) or sensitive (Red) to the RMS. X and Y axis displayed drug names and corresponding signaling pathways, respectively. **(c)** Violin plot displaying mRNA levels of eight target antigens of ADC between normal tissues and BCa samples, and between RMS-low and -high BCa samples, respectively.

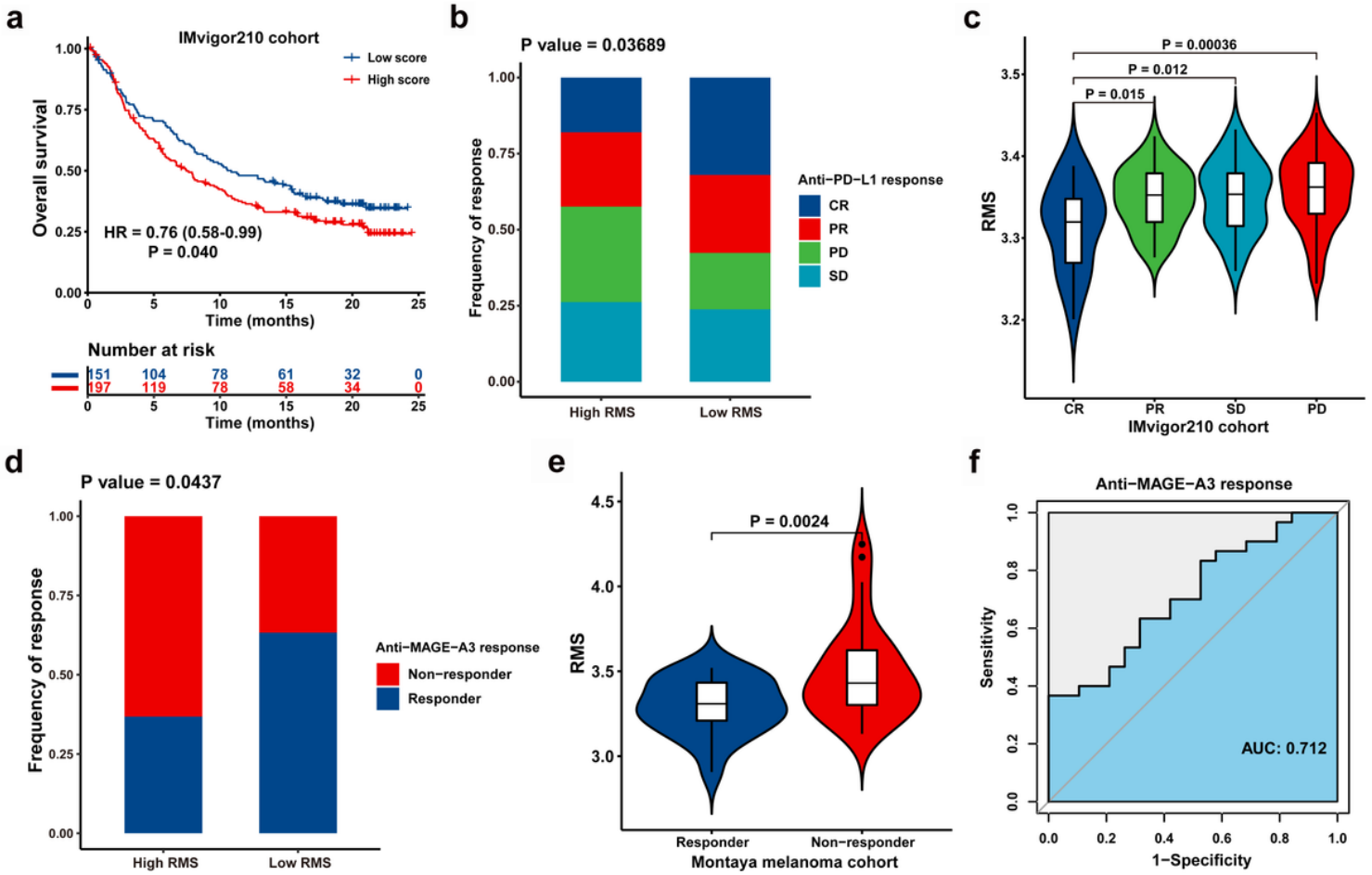

Figure 10

The association between the RMS and efficacy of immunotherapy in two cohorts. **(a)** Kaplan-Meier curve for OS of RMS-low and -high patients in IMvigor210 cohort. **(b)** Bar plot showing the fractions of different clinical responses to anti-PD-L1 immunotherapy in RMS-high or -low group in IMvigor210 cohort. **(c)** Violin plot displaying the distribution of the RMS in four groups about clinical response to anti-PD-L1 therapy in IMvigor210 cohort. **(d)** Bar plot revealing the proportions of different clinical responses to anti-MAGE-A3 immunotherapy in high/low RMS group in Montoya melanoma cohort. **(e)** Violin plot displaying the distribution of the RMS in four groups about clinical response to anti-MAGE-A3 treatment in Montoya melanoma cohort. **(f)** ROC curve describing the predictive performance of the RMS in evaluating patients' response to anti-MAGE-A3 immunotherapy in Montoya melanoma cohort.

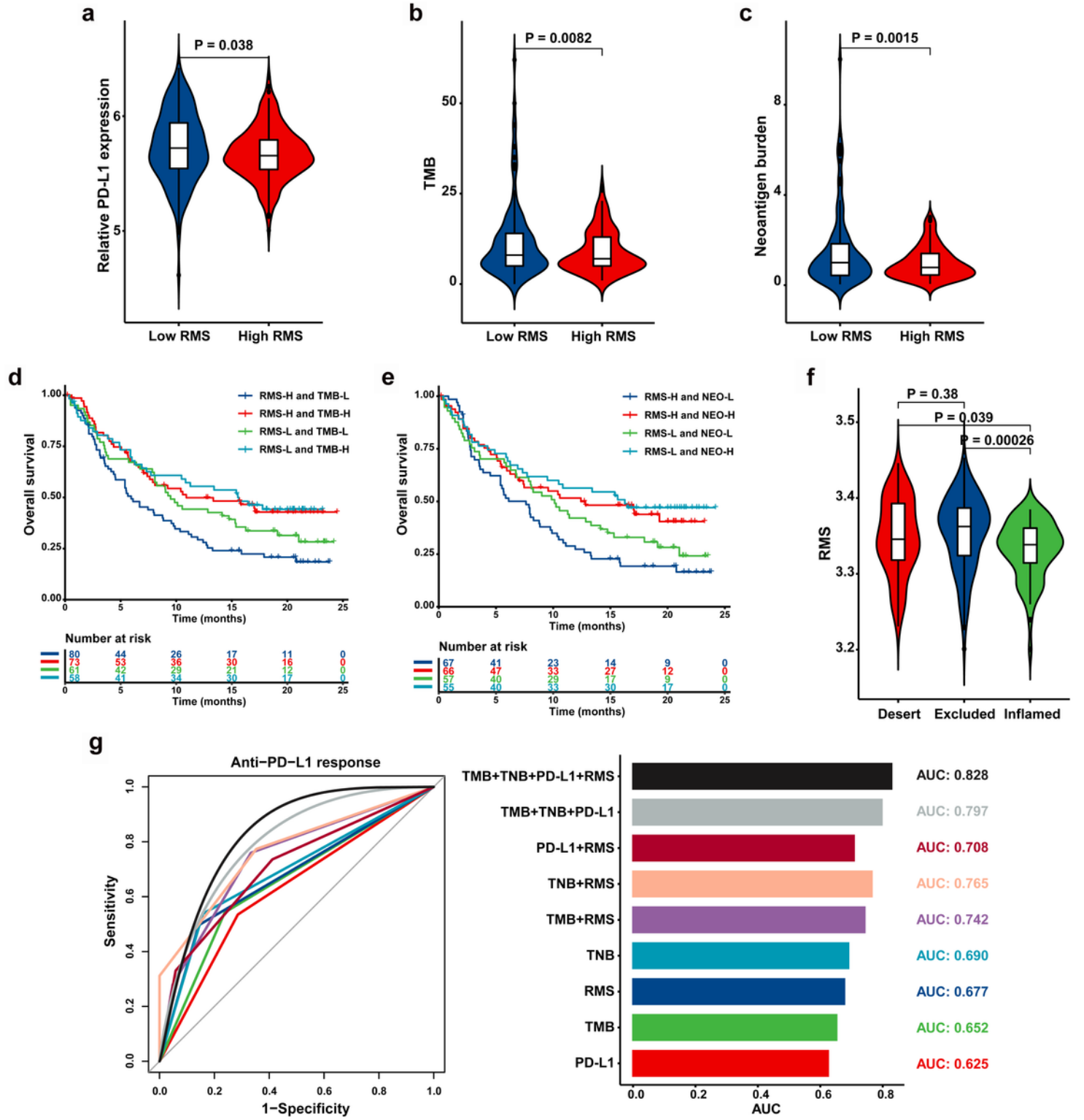

Figure 11

The biological significance and predictive value of RMS for the efficacy of anti-PD-L1 immunotherapy in IMvigor210 cohort. Violin plot depicting differences in the levels of **(a)** PD-L1, **(b)** TMB, and (**c**) neoantigen burden between RMS-low and -high group. Kaplan-Meier curve showing OS of multiple subgroups stratified by the RMS and (**d**) TMB or (**e**) neoantigen burden. (**f**) Violin plot presenting difference in the

RMS among three immune phenotypes. (**g**) Histogram and ROC curve displaying the predictive power of nine signatures composed of TMB, TNB, RMS and PD-L1.

Supplementary Files

This is a list of supplementary files associated with this preprint. Click to download.

- FigureS1.tif
- FigureS2.tif
- FigureS3.tif
- FigureS4.tif
- FigureS5.tif
- Supplementarytable.xlsx